

Beyond Nearest-neighbour Universality of Spectral Fluctuations in Quantum Chaotic and Complex Many-body Systems

Debojyoti Kundu,^{*} Santosh Kumar,[†] and Subhra Sen Gupta[‡]
*Department of Physics, Shiv Nadar Institution of Eminence (SNIOE),
 Gautam Buddha Nagar, Uttar Pradesh 201314, India*

Discerning chaos in quantum systems is an important problem as the usual route of Lyapunov exponents in classical systems is not straightforward in quantum systems. A standard route is the comparison of statistics derived from model physical systems to those from random matrix theory (RMT) ensembles, of which the most popular is the nearest-neighbour-spacings distribution (NNSD), which almost always shows good agreement with chaotic quantum systems. However, even in these cases, the long-range statistics (like number variance, spectral rigidity etc.), which are also more difficult to calculate, often show disagreements with RMT. As such, a more stringent test for chaos in quantum systems, via an analysis of intermediate-range statistics is needed, which will additionally assess the extent of agreement with RMT universality. In this paper, we deduce the effective level-repulsion parameters and the corresponding Wigner-surmise-like results of the next-nearest-neighbor spacing distribution (nNNSD) for integrable systems (semi-Poissonian statistics) as well as the three classical quantum-chaotic Wigner-Dyson regimes, by stringent comparisons to numerical RMT models and benchmarking against our exact analytical results for 3×3 Gaussian matrix models, along with a semi-analytical form for the nNNSD in the Orthogonal-to-Unitary symmetry crossover. To illustrate the robustness of these RMT based results, we test these predictions against the nNNSD obtained from quantum chaotic models as well as disordered lattice spin models. This reinforces the Bohigas-Giannoni-Schmit and the Berry-Tabor conjectures, extending the associated universality to longer range statistics. In passing, we also highlight the equivalence of nNNSD in the apparently distinct Orthogonal-to-Unitary and diluted-Symplectic-to-Unitary crossovers.

I. INTRODUCTION

Understanding and quantifying chaos in the quantum domain is a complex and topical problem [1–3]. The standard approach of testing for hyper-sensitivity to initial conditions via positive Lyapunov exponents in the classical domain [4, 5], does not work for quantum systems in any straightforward way due to ambiguity in the very concept of *trajectory*, in view of the uncertainty principle. The distinction of integrable systems vis-a-vis chaotic systems in quantum mechanics is a tricky problem [6], but a standard prescription has emerged over the years due to the seminal works of Berry and Tabor (Berry-Tabor conjecture) [7] on one hand, and Bohigas, Giannoni and Schmit (BGS conjecture) [8] on the other. These conjectures relate the local spectral fluctuations (e.g. NNSD) for quantum integrable systems to Poissonian statistics, and those of quantum chaotic systems to the statistics of the three standard Random Matrix Theory (RMT) Wigner-Dyson classes, further sub-classified according to the presence/absence of various anti-unitary (time-reversal) and unitary (spatial) symmetries [9, 10], respectively.

RMT was first introduced in Physics by Wigner to understand the statistical properties of neutron scatter-

ing spectra of heavy nuclei [11–13] and the mathematical framework and its connections to physical systems and their symmetries were further elucidated by the work of Wigner, Dyson, Porter, Mehta, Pandey and others [9, 14–24]. Over the years, RMT has seen an unprecedented number and variety of applications in Physics as well as in many inter-disciplinary subjects, ranging from disordered quantum many-body systems [1–3, 17, 18, 25–30], to large complex atoms, molecules, and quantum chaotic systems [1, 25, 29, 30], as also in finance, atmospheric science, medical science, and complex network theory [31–39].

In RMT, the study of the statistical behavior of the eigenspectra and eigenstates are of primary concern. The study of the eigenspectra involves the investigation of the *short-range* and the *long-range* spectral correlation properties. The investigation of *local* (short-range) fluctuations in the eigenspectrum often involves the analysis of two widely used measures: the *nearest-neighbor spacing distribution* (NNSD), which characterizes the probability distribution of spacings between consecutive eigenvalues, and the *ratio distribution* (RD), which examines the distribution of ratios of the consecutive level spacings [40–46]. The *spectral rigidity* (SD) and *number variance* (NV) measures are commonly employed to study the *global* (long-range) fluctuations in the eigenspectrum [47–52]. In the context of almost all spectral fluctuation measures, excluding those involving ratios of spacings, one usually needs to go through an *unfolding procedure* which scales the mean level spacing to unity, in order to compare spectral statistics from diverse physical systems to standard RMT classes. However, the unfolding

^{*} debojyoti.kundu.physics@gmail.com [Present Address : International Centre for Theoretical Sciences (ICTS) - TIFR, Bengaluru, India.]

[†] Corresponding Author : skumar.physics@gmail.com

[‡] Corresponding Author : subhro.sengupta@gmail.com

procedure of the eigenvalues is not unique [1, 25, 40, 42] and the long-range measures are extremely sensitive to the unfolding procedure [47, 51, 53]. Also, the presence of *finite-size effects* significantly affect these long-range measures for physical systems. In this context, the higher-order level spacing and ratio distribution studies may offer a more effective and numerically straightforward method to handle the *beyond-short-range* spectral correlations [41, 54–59].

The well-known Wigner-surmise results for NNSD of the three standard symmetry classes (GOE, GUE, and GSE), obtained from the joint probability distribution function (JPDF) of 2×2 Gaussian random matrices, serve as excellent approximations to the large-dimension exact results [1, 13, 17, 18, 25]. Similar results for RD, based on 3×3 matrix models, can also be found in Refs. [60–63]. To derive the exact Wigner-surmise-like results for higher-order level spacing and ratio distributions, one needs to deal with the higher dimensional JPDF's and the process become quite cumbersome. There are some early as well as recent studies [41, 54–59, 64, 65] which generalize these higher-order distributions by considering phenomenological and numerical fitting arguments.

In RMT, the Dyson index β is known to serve as the measure of the degree of level-repulsion in the eigenspectra of a system. An uncorrelated sequence of energy levels follow the Poissonian statistics with no level-repulsion ($\beta = 0$). The eigenspectra of the three Wigner-Dyson Gaussian ensembles, GOE, GUE, and GSE, possess finite degrees of level-repulsion and the corresponding $\beta = 1, 2,$ and $4,$ respectively. In these cases, the above values signify the number of independent *real* parameters in a typical *off-diagonal* element of the original matrix, that may be tweaked to control the degree of level-repulsion amongst its eigenvalues. For GOE, GUE and GSE, the off-diagonal elements being real numbers, complex numbers, and quaternions, thus have 1, 2 and 4 independently variable parameters, respectively. The higher-order level-spacing and ratio distributions, may also be expected to follow the generalized *Wigner-surmise-like* distributions [41, 55–59]. Therefore, one can identify *effective* Dyson indices, β' , corresponding to the degree of the level spacings of an ensemble.

The main objective of this paper is to establish a more stringent test for chaos in quantum systems, via an analysis of spectral statistics beyond NNSD, specifically the next-nearest-neighbour spacing distribution (nNNSD), for both the *integrable* as well as the *quantum chaotic* regimes. This is achieved by rigorous comparisons to a variety of physical systems, some with classically chaotic counterparts and some disordered quantum models with no classical counterpart, thus also assessing the extent of agreement with RMT universality. We deduce this based on the fitting of generalized Wigner surmise-like ansatzes for the nNNSD, to the eigenvalue statistics of large random matrices. To this end, we perform Monte-Carlo simulations of relevant random matrix models to determine the associated effective Dyson indices (β'), and con-

trasted with earlier studies [41, 56, 58, 59]. Furthermore, for the GOE and GUE, we present exact analytical expressions of the nNNSD's using the JPDF of eigenvalues of the corresponding 3×3 RMT matrix models. Also, using the JPDF of the 3×3 GOE-to-GUE crossover model, we derive a *semi-analytical* expression for the corresponding nNNSD crossover. The physical models used to examine the universality of these results include two single-body (non-interacting) quantum chaotic systems, namely the *quantum kicked rotor* (QKR) [66–70] and the *quarter Sinai billiard* [71–73], on one hand, and two many-body (interacting) disordered quantum systems, specifically two *disordered spin-chain models* [40, 47], on the other. *This corroborates the universality of the Berry-Tabor and BGS conjectures beyond nearest-neighbour spectral fluctuations for integrable as well as quantum chaotic systems with various possible symmetries.*

Towards the end, we also highlight the equivalence of nNNSD in the seemingly distinct GOE-to-GUE and *diluted*-GSE-to-GUE crossovers, where *diluted* refers to the case where both partners of all Kramers doublets are retained in the GSE spectra [47]. This is illustrated via an analysis of both RMT crossover matrix models as well as the two disordered, interacting lattice spin models. Despite having very different physical symmetry settings in two distinct spin models, it will be argued that both of them can be viewed, in a certain sense, as a transition between the NNSD of the standard GSE, and the nNNSD of the canonical GUE, based on the mathematical form of the distribution functions alone.

The rest of this paper is presented as follows. In Sec. II, we deduce the effective Dyson indices and thereby obtain the generalized Wigner-surmise expressions for the nNNSD's in the context of the integrable case as well as the three Wigner-Dyson ensembles, via a fitting procedure to Monte-Carlo simulations involving large-dimensional matrices. In Sec. III (supplemented by Appendix A), we consider the JPDF's of the eigenvalues of 3×3 random matrix models following GOE and GUE, and deduce the exact analytical results for the nNNSD's. These exact analytical results show good agreement with the generalized Wigner-surmise expressions obtained in Sec. II. Similarly, for the GOE-to-GUE nNNSD crossover, we derive a semi-analytical form and employ its numerical realizations for examining the limiting and intermediate cases. In Sec. IV, we investigate the QKR system in its integrable and strongly chaotic regimes (before and after breaking of the time-reversal symmetry), and study its nNNSD statistics. We also study the nNNSD's of the tight-binding (TB) Hamiltonian in both an *integrable rectangular billiard* and a *chaotic quarter Sinai billiard system* by using the computational package Kwant [74]. Here, we also introduce the aforementioned disordered spin-chain models (referred to as *model-I* and *model-II*), and explore the robustness of the previously deduced nNNSD results (in Sections II and III) by comparing them with the corresponding spectral statistics of these spin systems. Lastly, in Sec. V,

we discuss the equivalence of the two apparently distinct nNNSD crossovers as mentioned above. The key findings and conclusions are summarized in Sec. VI.

II. METHODOLOGY AND CALCULATIONS FOR RMT LEVEL SPACING DISTRIBUTIONS

The NNSD is the most studied short-range level correlation statistics, which represents the statistical behavior of the local fluctuations of an eigenspectrum. From the ordered sequence of the unfolded eigenvalues, $\tilde{\varepsilon}_1 \leq \dots \leq \tilde{\varepsilon}_j \leq \tilde{\varepsilon}_{j+1} \dots$, we can define the nearest-neighbor level spacing as $s_j = (\tilde{\varepsilon}_{j+1} - \tilde{\varepsilon}_j)$ [40]. The NNSD of uncorrelated energy levels follows the Poissonian statistics, as represented by

$$P_{\text{Poi}}(s) = \exp(-s). \quad (1)$$

On the other hand, the NNSD of correlated levels is given by the Wigner-surmise formula [1, 25]

$$P_{\text{WD}}(s) = a_\beta s^\beta \exp(-b_\beta s^2), \quad (2)$$

where β is the *Dyson index*, whose significance is described in the Introduction above. For example, $\beta = 1, 2,$ and 4 corresponds to the Gaussian orthogonal ensemble (GOE), Gaussian unitary ensemble (GUE), and Gaussian symplectic ensemble (GSE), respectively. The constants a_β and b_β , in Eq. (2), can be derived from the normalization and unit mean-level spacing conditions,

$$\int_0^\infty P_{\text{WD}}(s) ds = 1; \quad \int_0^\infty s P_{\text{WD}}(s) ds = 1. \quad (3)$$

The analytical NNSD formulas for the three Gaussian ensembles along with that for the Poissonian statistics are compiled in Table I.

Along similar lines, one can also consider higher order level spacings and study their corresponding distributions, assuming that they can also be represented by Wigner-surmise-like formulae with some *effective* β 's (denoted by β'). The probability distribution of the level spacings of a correlated spectra can be represented by the generalized Wigner-surmise formula [22, 41],

$$P_{\text{WD}}^m(w_m) = a_{\beta'} w_m^{\beta'} \exp(-b_{\beta'} w_m^2), \quad (4)$$

where m is the order of the level spacings and β' represents the corresponding *effective* Dyson index. Here, w_m is the m -th order level spacing of the unfolded eigenvalues [$(w_m)_j = (\tilde{\varepsilon}_{j+m} - \tilde{\varepsilon}_j)/m$] [41]. The $m = 1$ case represents the nearest-neighbor spacings s ($\equiv w_1$) and $m > 1$ represents higher order spacings. The constants, $a_{\beta'}$ and $b_{\beta'}$, can be derived from the corresponding normalization and unit mean-level spacing conditions,

$$\int_0^\infty P_{\text{WD}}^m(w_m) dw_m = 1; \quad \int_0^\infty w_m P_{\text{WD}}^m(w_m) dw_m = 1. \quad (5)$$

Table I. Probability distribution of nearest-neighbor spacings for unfolded eigenvalues [1, 25].

Type of distribution	NNSD Probability Density
Poissonian	$P_{\text{Poi}}(s) = \exp(-s)$
GOE	$P_{\text{GOE}}(s) = (\pi s/2) \exp(-\pi s^2/4)$
GUE	$P_{\text{GUE}}(s) = (32s^2/\pi^2) \exp(-4s^2/\pi)$
GSE	$P_{\text{GSE}}(s) = (2^{18}s^4/3^6\pi^3) \exp(-64s^2/9\pi)$

One can also generalize the probability distribution of the level spacings of an eigenspectrum, consisting of uncorrelated levels to higher order spacings, *i.e.* [64],

$$P_{\text{Poi}}^m(w_m) = c_{\beta'} w_m^{\beta'} \exp(-d_{\beta'} w_m), \quad (6)$$

where $\beta' = 0, m = 1$ represents the standard NNSD of the Poissonian statistics [$P_{\text{Poi}}(s)$], $c_{\beta'}$ and $d_{\beta'}$ can also be derived from the corresponding conditions as in Eq. (5).

It is known that the *next* nearest-neighbor spacing distribution of the Orthogonal (GOE) class has the exact same analytical form as the nearest-neighbor spacing distribution of the Symplectic (*standard* GSE) class [25, 27], *viz.*,

$$P_{\text{GOE}}^2(w_2) = (2^{18}/3^6\pi^3) w_2^4 \exp(-64w_2^2/9\pi), \quad (7)$$

where $(w_2)_j = (\tilde{\varepsilon}_{j+2} - \tilde{\varepsilon}_j)/2$ [42, 50] is the suitably normalized next nearest-neighbor level spacing ($m = 2$) of the unfolded eigenvalues. For other Wigner-Dyson ensembles, the analytical forms of the Wigner-surmise-like nNNSD's [$P_{\text{WD}}^2(w_2)$] are not widely known.

In this work, we address this issue based on a two-pronged approach. In the *first approach*, we assume a modified Poissonian or a modified Wigner-Dyson form for the nNNSD distribution functions as given by Eqs. (6) and (4), respectively, for the integrable and the quantum-chaotic cases, respectively. We then extract a form for the constants involved using the corresponding normalization conditions [Eq. (5)], which are still expressed in terms of the unknown index β' . This index is determined by detailed fittings to numerical diagonalization derived data for large matrices, as described below. In the *second approach* (discussed in the next section), we deduce exact formulas for the nNNSD distribution functions for the GOE and GUE classes based on an analytical treatment using the three-dimensional JPFD's for the eigenvalues.

To deduce the nNNSD of the integrable case (uncorrelated spectra), we need to solve for the constants $c_{\beta'}$ and $d_{\beta'}$, using Eq. (6) [$P_{\text{Poi}}^m(w_m)$] and the corresponding conditions in Eq. (5). We get,

$$c_{\beta'} = \frac{\Gamma(2 + \beta')^{1+\beta'}}{\Gamma(1 + \beta')^{2+\beta'}} = \frac{(1 + \beta')^{(1+\beta')}}{\Gamma(1 + \beta')},$$

$$d_{\beta'} = \frac{\Gamma(2 + \beta')}{\Gamma(1 + \beta')} = 1 + \beta', \quad (8)$$

where $\Gamma(z)$ is the *Euler Gamma* function. Next, we construct a numerical matrix (\mathcal{H}_{Poi}) of dimension $n = 15000$ (large n is considered to eliminate any possible finite-size

Table II. Probability distribution of next-nearest-neighbor spacings for unfolded eigenvalues.

Type of distribution	nNNSD Probability Density
Semi-Poissonian	$P_{\text{Poi}}^2(w_2) = 4w_2 \exp(-2w_2)$
GOE	$P_{\text{GOE}}^2(w_2) = (2^{18}/3^6\pi^3)w_2^4 \exp(-64w_2^2/9\pi)$
GUE	$P_{\text{GUE}}^2(w_2) = [5^8 7^8 \pi^4 / (2^{40} \times 3)] w_2^7 \exp(-5^2 7^2 \pi w_2^2 / 2^{10})$
GSE	$P_{\text{GSE}}^2(w_2) = [3^{12} 7^{14} 11^{14} 13^{14} \pi^7 / (2^{157} \times 5)] w_2^{13} \exp(-3^2 7^2 11^2 13^2 \pi w_2^2 / 2^{22})$

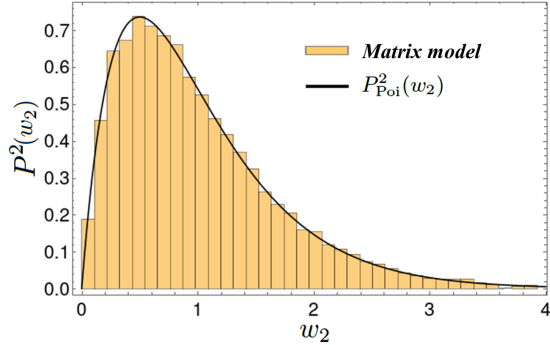


Figure 1. The nNNSD of the numerical matrix model matrix \mathcal{H}_{Poi} (dimension $n = 15000$) which has uncorrelated eigenvalues. The spacing distribution follows the semi-Poissonian distribution $P_{\text{Poi}}^2(w_2)$, mentioned in the Table II.

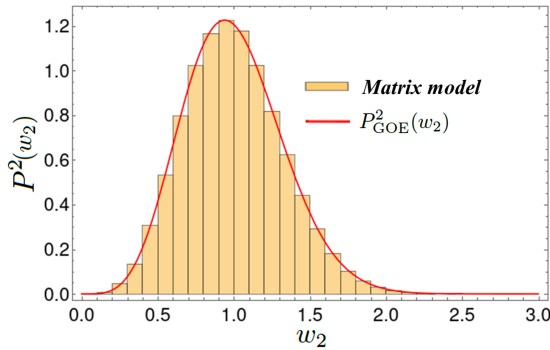


Figure 2. The nNNSD of the numerical random matrix model \mathcal{H}_{GOE} ($n = 10000$ and an ensemble of $\mathcal{M} = 20$ matrices), which perfectly follows the corresponding GOE distribution $P_{\text{GOE}}^2(w_2)$, mentioned in the Table II.

effects), whose eigenvalues are uncorrelated and NNSD follows Poissonian statistics. To obtain the parameter β' , we perform the *best fit* of the probability distribution function $P_{\text{Poi}}^2(w_2)$ [considering $c_{\beta'}$ and $d_{\beta'}$ in the form of Eq. (8)] to the nNNSD of the unfolded spectra of the constructed matrix \mathcal{H}_{Poi} . We find $\beta' = 1.006 \approx 1$, and using Eq. (8), the normalization constants become $c_1 = 4$ and $d_1 = 1$. This functional form, $P_{\text{Poi}}^2(w_2)$, mentioned in the Table II, is known as the *semi-Poissonian distribution*. [75] In Fig. 1, $P_{\text{Poi}}^2(w_2)$ is plotted along with the nNNSD *histogram* of the corresponding matrix model \mathcal{H}_{Poi} .

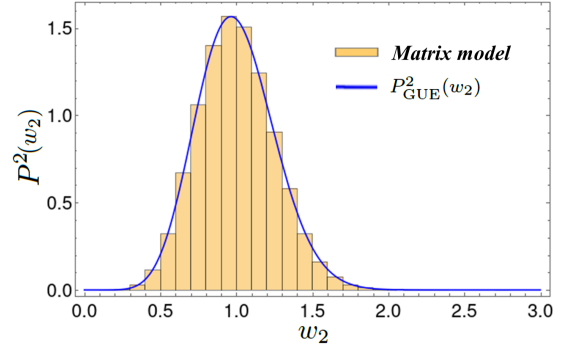


Figure 3. The nNNSD of the numerical random matrix model \mathcal{H}_{GUE} ($n = 40000$ and $\mathcal{M} = 5$), which perfectly follows the deduced GUE distribution $P_{\text{GUE}}^2(w_2)$, mentioned in the Table II.

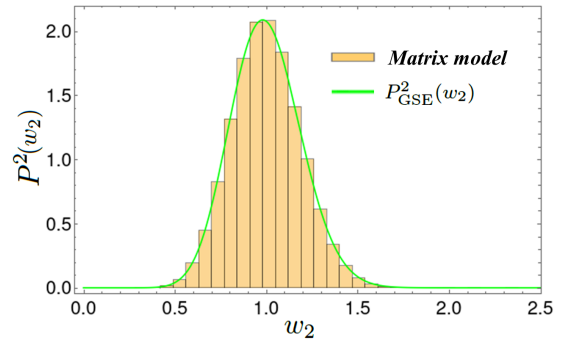


Figure 4. The nNNSD of the numerical random matrix model \mathcal{H}_{GSE} ($n = 40000$ and $\mathcal{M} = 5$), which perfectly follows the deduced GSE distribution $P_{\text{GSE}}^2(w_2)$, mentioned in the Table II.

In the same manner, to find out the analytical expressions of the nNNSD for the GOE, GUE and GSE classes, we solve for $a_{\beta'}$ and $b_{\beta'}$, using Eq. (4) [$P_{\text{WD}}^m(w_m)$] and the corresponding conditions in Eq. (5). We get the generic expressions:

$$a_{\beta'} = \frac{2(b_{\beta'})^{\left(\frac{1+\beta'}{2}\right)}}{\Gamma\left(\frac{1+\beta'}{2}\right)}, \quad b_{\beta'} = \frac{[\Gamma(1+\frac{\beta'}{2})]^2}{[\Gamma(\frac{1+\beta'}{2})]^2}. \quad (9)$$

Then, we construct numerical Gaussian random matrices (\mathcal{H}_{WD}) of dimension n ($= 10000, 40000$, and 40000 for the GOE, GUE, and GSE, respectively), from the respective RMT ensembles following Wigner-Dyson symmetry classes. For these symmetry classes, we sample the matrices using ensemble sizes of $\mathcal{M} = 20, 5$, and 5 , for the GOE, the GUE, and the GSE, respectively. The standard

unfolding procedure is carried out before computing the probability distributions of the level spacings. For each case, we perform the *best fit* of the distribution $P_{\text{WD}}^2(w_2)$ [Eq. (4) with $m = 2$ and considering $a_{\beta'}$ and $b_{\beta'}$ in the form of Eq. (9)] to the respective nNNSD of the eigenvalues of the RMT matrix models and obtain the corresponding effective Dyson index, β' . As expected, for the GOE class, using \mathcal{H}_{GOE} , we get the parameter $\beta' = 3.996 \approx 4$, and we solve for a_4 and b_4 using the Eq. (9). We achieve the analytical form presented in Eq. (7) [$P_{\text{GOE}}^2(w_2)$], which is also equivalent to the corresponding NNSD of the standard GSE [25]. For the GUE class, using \mathcal{H}_{GUE} , we get $\beta' = 7.002 \approx 7$. And using \mathcal{H}_{GSE} , we find that the nNNSD of the GSE class has a value $\beta' = 13.015 \approx 13$. The agreement of our computed effective Dyson index values for the nNNSD of the three Gaussian ensembles with those deduced in Refs. [56, 58, 59], based on heuristic arguments and numerical studies, reasserts the scaling relations proposed therein. We observe that, the values of the effective Dyson indices β' , are *universal*, i.e., they depend on the nature of the RMT ensembles, not on the kind of spectral statistic studied.

With the normalization conditions taken care of, using Eq. 9, we compile the values for the normalizing constants for the all symmetry classes, and based on these values, compile the Wigner-surmise-like formulas for the nNNSD distribution functions in Table II. The nNNSD *histograms* of the matrix models (\mathcal{H}_{WD}), along with the corresponding best-fitted $P_{\text{WD}}^2(w_2)$ distributions (from Table II) are plotted in Figs. 2 (GOE), 3 (GUE), and 4 (GSE), respectively. For comparison, the Wigner-surmise-like functional forms for the nNNSD's (as summarized in Table II) for the integrable case (semi-Poissonian) along with all the Wigner-Dyson ensembles, are plotted in Fig. 5(b). A similar comparison for NNSD's is also plotted in Fig. 5(a). We find that, just as for the NNSD, the nNNSD for the Wigner-Dyson classes also show signs of increasing level-repulsion as one goes from GOE to GUE to GSE, as depicted by the shifting of the peaks of the distribution functions towards higher values of w_2 , in that order. Also the distribution function is zero at $w_2 = 0$ (degeneracies not favored) and remains very small till about $w_2 = 0.25$, which is somewhat larger than the thresholds for the NNSD case, as also borne out by the much larger leading powers of w_2 in these expressions (for small w_2 , see Table II) compared to

those for the NNSD's (see Table I). But more strikingly, even for the integrable case, the probability is no longer large for $w_2 = 0$, but actually zero. However, since in the integrable case, the eigenlevels are uncorrelated, this just implies that not more than two consecutive levels coincide [58]. This is unlike the correlated cases of random matrix ensembles, where level repulsion arises due to the *Vandermonde factor* [25], which involves the product of differences between eigenvalues and leads to a vanishing probability density at zero spacing.

In the following section, we present exact analytical expressions for the next nearest-neighbor spacing distributions based on 3×3 matrix models and derive a semi-analytical interpolation distribution between Gaussian orthogonal and Gaussian unitary ensembles using three-dimensional joint probability densities.

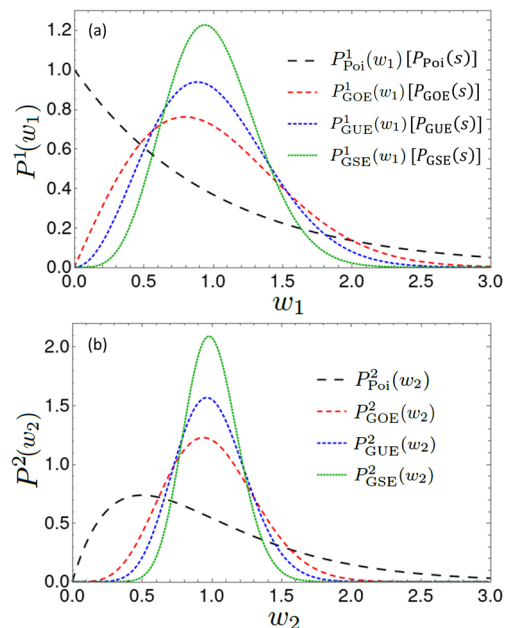


Figure 5. The comparison between the nearest-neighbor and next nearest-neighbor spacing distributions; (a) presents the comparison between the Wigner-surmise functional forms for the NNSD's of the Poissonian statistics, and the three WD ensembles (see the expressions in the Table I), (b) presents the comparison between the Wigner-surmise-like functional forms for the nNNSD's of the semi-Poissonian statistics, and the three WD ensembles (see the expressions in the Table II).

III. EXACT nNNSD RESULTS FOR 3×3 GAUSSIAN RANDOM MATRICES

Similar to Wigner-surmise formulae, which are based on 2×2 matrix models, one may employ 3×3 matrix models to deduce analytical expressions for the nNNSD. These expressions serve as an alternative to the Wigner-surmise results based on effective- β (β') and are capable of effectively approximating large-dimensional cases while also offering valuable additional insights. Notably, analytical expressions for the nNNSD are already known for GOE and GUE due to Porter and Kahn [20–22]. Here, we present the scaled versions of these distributions which ensure

both the overall unit-normalization and the unit mean-nNNSD conditions. For completeness, in the Appendix, the corresponding derivations are included. Additionally, we tackle the GOE-to-GUE crossover using the joint probability densities of three-dimensional Gaussian matrix ensembles and obtain semi-analytical results which can be used to capture the orthogonal-to-unitary crossover in physical systems by relating the generic RMT crossover parameter to various physical symmetry-breaking parameters, under different circumstances.

A. Exact Analytical Results of nNNSD for GOE and GUE

We present the probability density for the GOE [from Eq. (A7) in the Appendix],

$$\mathcal{Q}_{\text{GOE}}(\mathfrak{s}) = \frac{3^4 \exp(-9\mathfrak{s}^2/\pi) \mathfrak{s} \left(6\mathfrak{s} - \exp(9\mathfrak{s}^2/4\pi) (2\pi - 9\mathfrak{s}^2) \operatorname{erf}\left[\frac{3\mathfrak{s}}{2\sqrt{\pi}}\right]\right)}{4\pi^2}, \quad (10)$$

where the \mathfrak{s} is the scaled next nearest-neighbor spacing variable and $\operatorname{erf}[z] = \frac{2}{\sqrt{\pi}} \int_0^z e^{-t^2} dt$ is the *error function*. Also, the probability density for GUE is given by [Eq. (A8)]

$$\mathcal{Q}_{\text{GUE}}(\mathfrak{s}) = \frac{3^{11} \sqrt{3} \exp(-3^5 \mathfrak{s}^2 / 2^4 \pi) \mathfrak{s}^2 \left(2^3 3^3 \mathfrak{s} (-2^5 \pi + 3^4 \mathfrak{s}^2) + \sqrt{3} \exp(3^5 \mathfrak{s}^2 / 2^6 \pi) (2^{10} \pi^2 - 2^6 3^4 \pi \mathfrak{s}^2 + 3^9 \mathfrak{s}^4) \operatorname{erf}\left[\frac{9}{8} \sqrt{\frac{3}{\pi}} \mathfrak{s}\right]\right)}{2^{20} \pi^4}. \quad (11)$$

As mentioned in the Appendix, the scaled parameter \mathfrak{s} is formally equivalent to the parameter w_2 . So, to compare the Wigner-surmise-like results, $P_{\text{GOE}}^2(w_2)$ and $P_{\text{GUE}}^2(w_2)$, against the exact analytical distributions, $\mathcal{Q}_{\text{GOE}}(\mathfrak{s}) [\equiv \mathcal{Q}_{\text{GOE}}(w_2)]$ and $\mathcal{Q}_{\text{GUE}}(\mathfrak{s}) [\equiv \mathcal{Q}_{\text{GUE}}(w_2)]$, respectively, we perform their Taylor expansion about $w_2 = 1$, around which point they possess maximum probability. For the GOE case, the expansion up to third order gives,

$$\lim_{w_2 \rightarrow 1} P_{\text{GOE}}^2(w_2) = 1.206 - 0.635(w_2 - 1) - 4.974(w_2 - 1)^2 + 4.288(w_2 - 1)^3 + \dots \quad (12)$$

and

$$\lim_{w_2 \rightarrow 1} \mathcal{Q}_{\text{GOE}}(w_2) = 1.201 - 0.650(w_2 - 1) - 4.908(w_2 - 1)^2 + 4.361(w_2 - 1)^3 + \dots, \quad (13)$$

and for the GUE,

$$\lim_{w_2 \rightarrow 1} P_{\text{GUE}}^2(w_2) = 1.551 - 0.801(w_2 - 1) - 11.051(w_2 - 1)^2 + 9.398(w_2 - 1)^3 + \dots \quad (14)$$

and

$$\lim_{w_2 \rightarrow 1} \mathcal{Q}_{\text{GUE}}(w_2) = 1.546 - 0.817(w_2 - 1) - 10.922(w_2 - 1)^2 + 9.527(w_2 - 1)^3 + \dots. \quad (15)$$

By examining Eqs. (12) and (13) for the GOE and Eqs. (14) and (15) for the GUE, we observe that the maximum difference between the coefficients in the Taylor expansion of the Wigner-surmise-like results and the corresponding exact analytical results, ranges between 10^{-3} to 10^{-1} . To add more credibility to our line of reasoning, in Fig. 6(a), we compare $P_{\text{GOE}}^2(w_2)$ [$P_{\text{GUE}}^2(w_2)$] against the exact analytical distribution $\mathcal{Q}_{\text{GOE}}(\mathfrak{s})$ [$\mathcal{Q}_{\text{GUE}}(\mathfrak{s})$]. We observe that, the corresponding distributions match very well, which can also be confirmed from the extremely small values ($\sim 10^{-5}$) of their Kullback-Leibler (KL) divergences [40], [$D_{KL}(P_{\text{GOE}}^2 \parallel \mathcal{Q}_{\text{GOE}})$ and $D_{KL}(P_{\text{GUE}}^2 \parallel \mathcal{Q}_{\text{GUE}})$], respectively, which measures the similarity of the two probability distributions, as a whole. Next, we derive a semi-analytical interpolating distribution for the GOE-to-GUE crossover.

B. Derivation of Semi-analytical Result for nNNSD in GOE-to-GUE Crossover

To start with, we consider the well known form of the Pandey-Mehta crossover matrix model [23, 24, 63, 76]:

$$\mathcal{H} = \sqrt{1 - \gamma^2} \mathcal{H}_0 + \gamma \mathcal{H}_1, \quad (16)$$

where the crossover parameter γ is varied from 0 to 1 and leading to an interpolation between the two RMT ensembles having characteristic Hamiltonians \mathcal{H}_0 and \mathcal{H}_1 , respectively. For our purpose, we consider the GOE-to-GUE crossover matrix model:

$$\mathcal{H}_{\text{GOE-GUE}} = \sqrt{1 - \gamma^2} \mathcal{H}_{\text{GOE}} + \gamma \mathcal{H}_{\text{GUE}}, \quad (17)$$

which interpolates between the GOE and GUE symmetry classes.

Now, from the Refs. [23–25, 63], we get the analytical expression of the joint probability distribution function for the GOE-to-GUE crossover, $p_\gamma(x_1, x_2, x_3)$, which uses the three-dimensional crossover matrix model $\mathcal{H}_{\text{GOE-GUE}}$ [Eq. (17)], and given by

$$p_\gamma(x_1, x_2, x_3) = \frac{1}{48\sqrt{2\pi}(1-\gamma^2)^{3/2}} [f(x_1-x_2) + f(x_2-x_3) - f(x_1-x_3)] (x_1-x_2)(x_2-x_3)(x_1-x_3) e^{-\frac{1}{4}(x_1^2+x_2^2+x_3^2)}, \quad (18)$$

where $f(u) = \text{erf} \left[\left(\frac{1-\gamma^2}{8\gamma^2} \right)^{1/2} u \right]$. Now, using Eq. (A4), we get

$$F_\gamma(\mathfrak{s}) = 6 \int_{-\infty}^{\infty} dx_2 \int_{-\infty}^{x_2} dx \int_{x_2}^{\infty} dy p_\gamma(x_2-x, x_2, x_2+y) \delta[\mathfrak{s} - (x+y)], \quad (19)$$

and after integrating over x_2 , we are left with

$$F_\gamma(\mathfrak{s}) = \frac{1}{4\sqrt{6\pi}(1-\gamma^2)^{3/2}} \int_0^\infty dx \int_0^\infty dy e^{-\frac{(x^2+xy+y^2)}{6}} xy(x+y) [f(x) + f(y) - f(x+y)] \delta[\mathfrak{s} - (x+y)]. \quad (20)$$

After performing the integration over y , we get the semi-analytical distribution for GOE-to-GUE interpolation as

$$F_\gamma(\mathfrak{s}) = \frac{1}{4\sqrt{6\pi}(1-\gamma^2)^{3/2}} \int_0^\mathfrak{s} dx e^{-\frac{(-s^2+sx-x^2)}{6}} \mathfrak{s}(\mathfrak{s}-x)x [f(x) + f(\mathfrak{s}-x) - f(\mathfrak{s})]. \quad (21)$$

Unfortunately, the above integration cannot be evaluated in a closed analytical form, therefore, we adopt a *semi-analytical* approach. We consider the integrand in the above equation as the density

$$f_\gamma(\mathfrak{s}, x) = \frac{1}{4\sqrt{6\pi}(1-\gamma^2)^{3/2}} e^{-\frac{(-s^2+sx-x^2)}{6}} \mathfrak{s}(\mathfrak{s}-x)x [f(x) + f(\mathfrak{s}-x) - f(\mathfrak{s})], \quad (22)$$

and then numerically evaluate the integral for different values of the crossover parameter γ . Next, we also need to normalize $F_\gamma(\mathfrak{s})$ for each values of γ . For example, for the $\gamma = 1/2$ case, $\int_0^\infty d\mathfrak{s} \int_0^\mathfrak{s} f_{\gamma=1/2}(\mathfrak{s}, x) dx = 1$ and $\int_0^\infty \mathfrak{s} d\mathfrak{s} \int_0^\mathfrak{s} f_{\gamma=1/2}(\mathfrak{s}, x) dx = 4.52873 = \kappa$. Now, we get the corresponding normalized nNNSD function with unit mean density, as $\mathcal{F}_{\gamma=1/2}(\mathfrak{s}) = \kappa F_{\gamma=1/2}(\kappa\mathfrak{s})$. Similarly, we get $\mathcal{F}_\gamma(\mathfrak{s})$ for various values of the crossover parameter γ .

In Fig. 6(b), we plot the semi-analytical interpolating distribution $\mathcal{F}_\gamma(\mathfrak{s})$ for the GOE-to-GUE crossover. The limiting distributions, $\mathcal{F}_{\gamma=0.001}(\mathfrak{s})$ ($\gamma \rightarrow 0$) and $\mathcal{F}_{\gamma=0.999}(\mathfrak{s})$ ($\gamma \rightarrow 1$), match well with $P_{\text{GOE}}^2(w_2)$ and $P_{\text{GUE}}^2(w_2)$, respectively. We also plot one of the intermediate cases, $\mathcal{F}_{\gamma=1/2}(\mathfrak{s})$, which lies between the limiting distributions. In the next section, we study the robustness of all the nNNSD results obtained both in this section and in the previous Sec. II, by comparing them against the corresponding distributions in a single-body and two many-body quantum chaotic systems.

IV. STUDY OF nNNSD IN PHYSICAL SYSTEMS

In view of the discussions in the previous sections, and applications of NNSD universality to various physical systems [40, 42–47], based on the standard Berry-Tabor [7] and BGS [8] conjectures, it is expected that the emergence of the nNNSD Statistics as shown by the Wigner-surmise-like results of Table II and also embodied by the *exact* Eqs. (10) and (11), should also be indicative of whether a model physical system is integrable or ergodic (chaotic), thus generalising the results of the aforesaid conjectures. To test this and check the robustness of the nNNSD universality and their extent of agreement with the spectral statistics of physical systems, we now proceed to study several physical systems

and compare their eigenvalue statistics with the results derived above. Specifically we study four diverse systems in all. The first two are non-interacting single-body models with well-known classically integrable and chaotic limits. These are the Quantum Kicked Rotor (QKR) and the Quantum Quarter Sinai Billiard (QQSB). The latter two systems are two different models of interacting spin- $\frac{1}{2}$'s on a 1D lattice, which have no classical counterpart whatsoever.

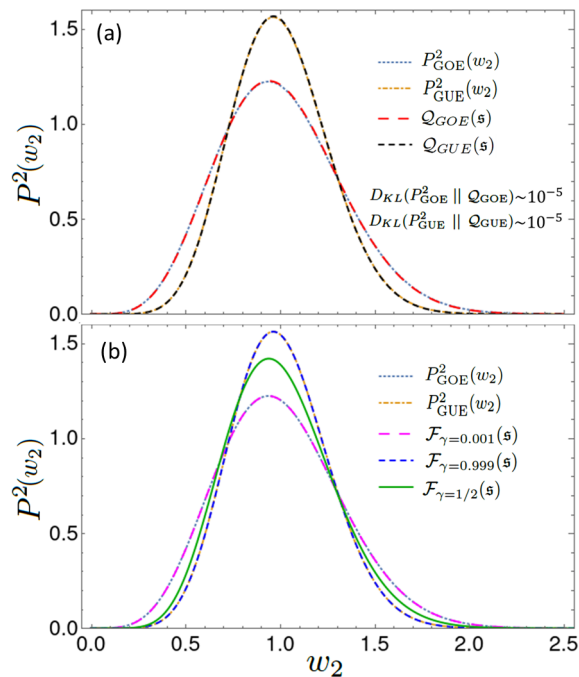


Figure 6. Comparison in nNNSD results. (a) shows comparison between the Wigner-surmise-like distribution $P^2_{GOE}(w_2)$ [$P^2_{GUE}(w_2)$] and the analytical distribution $Q_{GOE}(s)$ [$Q_{GUE}(s)$], derived from the three-dimensional JPDF of eigenvalues. They show excellent agreement, as is also borne out by the very small ($\sim 10^{-5}$) values of the KL divergence measures [$D_{KL}(P^2_{GOE} \parallel Q_{GOE})$ and $D_{KL}(P^2_{GUE} \parallel Q_{GUE})$] between them. In (b), the semi-analytical distribution $F_{\gamma}(s)$ is plotted which beautifully interpolates between GOE and GUE limits for the nNNSD.

A. Non-interacting Quantum Systems with Well-known Classically Chaotic Limits

1. The Quantum Kicked Rotor (QKR)

It is well-known that in 1D systems which are conservative, no chaos is possible as there is one degree of freedom and one conserved quantity (energy). So the only way to overcome this is to break the energy conservation by introducing a time-dependent term with a tunable amplitude so that the integrability may be broken gradually. In addition, if the time-dependent term is periodic in time, although energy is not strictly conserved, a discretized *quasi-energy* is conserved, much akin to the conservation of lattice momentum in spatially periodic crystals. The kicked rotor system is a well-known prototype of the above kind, and a single-body chaotic model that has been investigated in both classical [77, 78] and quantum regimes [66–68, 79, 80]. The NNSD of the quantum kicked rotor system follows the universal Wigner-Dyson distributions in the strongly chaotic limit [66, 68, 80, 81]. In this section, we investigate the nNNSD of the QKR system.

In a kicked rotor, a particle is confined to a ring (peri-

odic boundary conditions) and exposed to periodic kicks that vary with its angular position (θ). In order to also simulate the GUE regime via the breaking of *time-reversal symmetry*, we have introduced an effective magnetic field via a minimal-coupling like term (η) in the kinetic energy term. The Hamiltonian of the kicked rotor system is given by [63, 67–69, 79]

$$H_{KR} = \frac{(p + \eta)^2}{2} + \alpha \cos(\theta + \theta_0) \sum_{m=-\infty}^{\infty} \delta(t - m), \quad (23)$$

where p represents the angular momentum operator and α is the *kicking* (or *stochasticity*) parameter. The quantity θ_0 is the *parity* breaking parameter and η ($0 \leq \eta < 1$) is the *time-reversal* symmetry breaking parameter. The Dirac comb [$\sum_{m=-\infty}^{\infty} \delta(t - m)$] is employed to deliver periodic kicks to the particle at integer time intervals ($t = m$). Using Floquet's theorem [1], the unitary *time evolution* operator $U = BG$, guides the quantum dynamics of the QKR system, where, $B(\alpha) = \exp[-\frac{i}{\hbar} \alpha \cos(\theta + \theta_0)]$ is a function of the *kicking* parameter α , and $G = \exp[-\frac{i}{2\hbar} (p + \eta)^2]$ [69, 70, 81]. Under the *torus* boundary condition, the position (θ) and momentum (p) operators give discrete eigenvalues and U is reduced to a finite $\mathcal{N} \times \mathcal{N}$ dimensional matrix form. The position representations of B and G are [63, 66, 69, 70, 80]

$$B_{kl} = \exp\left[-i\alpha \cos\left(\frac{2\pi k}{\mathcal{N}} + \theta_0\right)\right] \delta_{kl} \quad (24)$$

and

$$G_{kl} = \frac{1}{\mathcal{N}} \sum_{j=-\frac{(\mathcal{N}-1)}{2}}^{\frac{(\mathcal{N}-1)}{2}} \exp\left[-i\left(\frac{j^2}{2} - \eta j - 2\pi j \frac{(k-l)}{\mathcal{N}}\right)\right], \quad (25)$$

where $k, l = -(\mathcal{N}-1)/2, -(\mathcal{N}-1)/2 + 1, \dots, (\mathcal{N}-1)/2$ and we set $\hbar = 1$. From this, it is clear that the indices (k, l) are equivalent to the magnetic quantum number $m_{\mathcal{J}}$ (where \mathcal{J} is the value of the angular momentum involved) and $\mathcal{N} = (2\mathcal{J} + 1)$ is the degeneracy of that level. Evidently for large values of \mathcal{N} the system should exhibit semi-classical behavior. In the position basis, the kl -th element of the unitary matrix of the time evolution operator becomes [63, 66, 69, 70, 80]

$$U_{kl} = \frac{1}{\mathcal{N}} \exp\left[-i\alpha \cos\left(\frac{2\pi k}{\mathcal{N}} + \theta_0\right)\right] \times \sum_{j=-\frac{(\mathcal{N}-1)}{2}}^{\frac{(\mathcal{N}-1)}{2}} \exp\left[-i\left(\frac{j^2}{2} - \eta j - 2\pi j \frac{(k-l)}{\mathcal{N}}\right)\right]. \quad (26)$$

The eigenvalues of the unitary matrix U are phase factors of the form $e^{i\varphi_j}$ and they lie on a unit circle. The ordered sequence of the *eigenangles*, $0 \leq \varphi_1 < \varphi_2 < \dots < \varphi_{\mathcal{N}_1} < 2\pi$, are considered to study the level spacing distributions for the QKR system. Using the unfolded

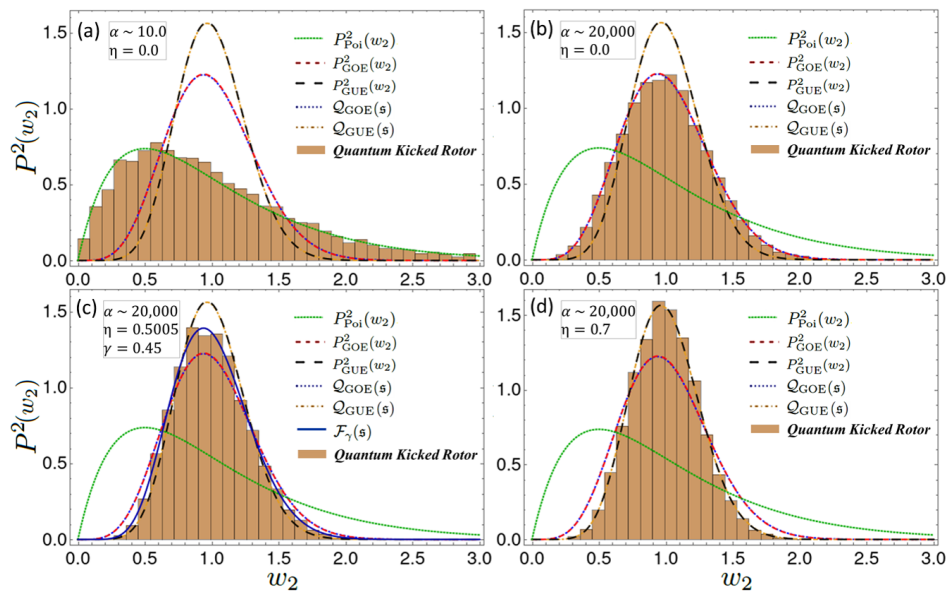


Figure 7. The nNNSD's of eigenangles for the single-body QKR system. (a) Shows that the nNNSD of the QKR system faithfully follows the semi-Poissonian distribution $[P_{\text{Poi}}^2(w_2)]$ for $\alpha \sim 10$. In (b) and (d), we plot the nNNSD, for the QKR system, in the GOE limit ($\eta = 0$) and GUE limit ($\eta = 0.7$), respectively. They follow the corresponding Wigner-surmise-like expressions, $P_{\text{GOE}}^2(w_2)$ and $P_{\text{GUE}}^2(w_2)$, as also by the exact analytical distributions, $\mathcal{Q}_{\text{GOE}}(\mathfrak{s})$ and $\mathcal{Q}_{\text{GUE}}(\mathfrak{s})$, as expected. In (c), the intermediate distribution ($\eta = 0.5005$), in the crossover region, is also seen to be perfectly reproduced by our derived semi-analytical distribution $\mathcal{F}_\gamma(\mathfrak{s})$ with $\gamma = 0.45$.

eigenangles $[\tilde{\varphi}_j = \varphi_j(\mathcal{N}/2\pi)]$, we can define the next-nearest neighbor spacings $(w_2)_j = (\tilde{\varphi}_{j+1} - \tilde{\varphi}_j)/2$. Even though the classical kicked rotor system exhibits chaotic motion when subjected to a relatively low kicking parameter ($\alpha \sim 10$), the NNSD of the QKR system still adheres to Poissonian statistics. This can be attributed to the presence of localization effects [69, 79, 81–84]. When the parity symmetry is fully broken ($\theta_0 = \pi/2\mathcal{N}$), and the kicking parameter α is very large ($\alpha^2 \gg \mathcal{N}$), the time-reversal symmetry of the QKR system is *preserved* (*broken*) for $\eta = 0$ ($\eta \neq 0$) and the level correlation statistics follows the universal GOE (GUE) distribution [69, 70, 81].

In Fig. 7(a), we examine the nNNSD in the QKR system with $\alpha \sim 10$ (integrable limit) and for an ensemble of $\mathcal{M} = 20$ matrices [85], for $\mathcal{N} = 501$ and observe its semi-Poissonian behavior. In Fig. 7(b)-(d), we present the nNNSD of the QKR system in the quantum chaotic regime with $\alpha \sim 2 \times 10^4$ ($\mathcal{M} = 20\text{VI}$ and $\mathcal{N} = 501$). Fig. 7(b) represents the time-reversal symmetry invariant QKR system with $\eta = 0$ [69, 70, 81] and the plotted nNNSD follows the Wigner-surmise-like distribution $P_{\text{GOE}}^2(w_2)$, as one might expect. We also notice that, the *exact* distribution for GOE, $\mathcal{Q}_{\text{GOE}}(\mathfrak{s})$, matches well with the spectral correlation statistics of the quantum chaotic system, in this limit. Similarly, for a time-reversal symmetry broken QKR system ($\eta = 0.7$) [69, 70], we plot the nNNSD in Fig. 7(d), and it follows the distribution $P_{\text{GUE}}^2(w_2)$, quite closely. Also, the time-reversal symmetry broken QKR system seems to follow the *exact* analytical distribution $\mathcal{Q}_{\text{GUE}}(\mathfrak{s})$ for the nNNSD (GUE

regime), as one would expect. In Fig. 7(c), we plot an intermediate (partially symmetry-broken) case with $\eta = 0.5005$, which can be perfectly mapped by our derived semi-analytical distribution $\mathcal{F}_\gamma(\mathfrak{s})$ with $\gamma = 0.45$.

2. The Quantum Quarter Sinai Billiard (QQSB)

Next we proceed to a family of non-interacting systems in 2D, namely the Quantum Billiards [8, 66, 71–73, 86–94], which have classically integrable or chaotic counterparts. In two dimensions, integrability requires the conservation of one more quantity, in addition to energy, so that even conservative systems may exhibit chaos, under suitable conditions. For example, in a circular billiard, both energy and the component of angular momentum along the perpendicular axis through the center are conserved, and it shows no chaos. But for a Sinai billiard [71–73] (square or rectangular shape, with a circular or elliptic hole cut out at the center), or for a Bunimovich stadium [73, 87, 88], angular momentum is no longer conserved and a chaotic regime is possible.

Thus, the quantum billiard systems are potential single-body quantum-chaotic systems which have classically chaotic counterparts [8, 66, 71–73, 86–94]. The nearest-neighbor spectral fluctuation statistics of quantum chaotic billiards has been widely explored by RMT studies, pioneered by the ground-breaking work of Bohigas, Giannoni and Schmit in the famous BGS Conjecture paper [8]. One such system is the *quarter Sinai billiard*

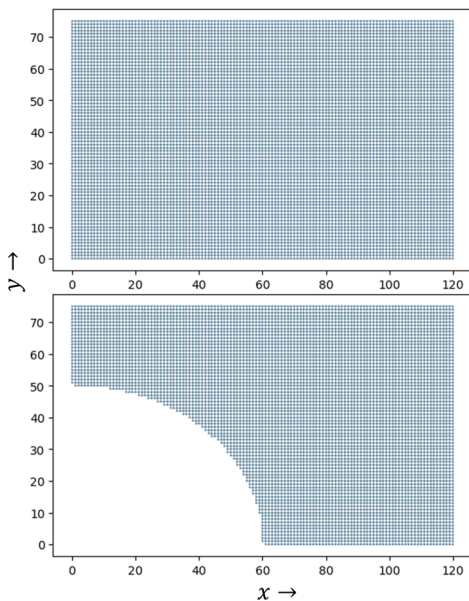


Figure 8. Top: the Kwant-generated schematic of an integrable rectangular billiard with dimension 120×75 and the corresponding tight-binding matrix dimension is 9196. Bottom: the schematic of a quarter Sinai billiard system, represented in a 120×75 rectangular lattice using Kwant by removing a *quarter* elliptical shape from the lower left corner. The elliptical shape follows the equation $x^2/60^2 + y^2/50^2 = 1$. The dimension of the corresponding tight-binding matrix is 6789.

[71–73]. In this study, we employ Kwant [74], an open source computational tool, to analyze the nNNSD’s of the discretized version of the tight-binding (TB) Hamiltonian in the two-dimensional quarter Sinai billiard system, operating in the chaotic regime. The discretized tight-binding model Hamiltonian is given by [73, 74]

$$H_{TB} = \sum_{ij} [(V(ak, al) + 4t) |k, l\rangle \langle k, l| - t(|k+1, l\rangle \langle k, l| + |k, l\rangle \langle k+1, l| + |k, l+1\rangle \langle k, l| + |k, l\rangle \langle k, l+1|)], \quad (27)$$

where $t = \hbar^2/(2ma^2)$ is the hopping parameter with a as the lattice constant and m as the mass of the particle. $|k, l\rangle$ ($\equiv |ak, al\rangle = |x, y\rangle$) represent the discretized positional states corresponding to the potential $V(x, y)$.

If one applies a time-reversal symmetry breaking, uniform magnetic field to the system, it modifies the hopping term t by introducing an additional phase factor, $\exp[-\frac{ie}{\hbar c} \int_{\mathbf{r}_1}^{\mathbf{r}_2} d\mathbf{r} \cdot \mathbf{A}(\mathbf{r})]$, known as the Peierls or the Aharonov-Bohm phase, where $\mathbf{A}(\mathbf{r})$ is the corresponding vector potential. We use the Peierls substitution scheme [73, 74, 95, 96] in the Kwant code to implement the hopping between two lattice points, \mathbf{r}_1 and \mathbf{r}_2 . For the two-dimensional billiard, a choice of gauge, $\mathbf{A} \equiv (A_x, A_y, A_z) \equiv (-By, 0, 0)$, ensures the constant and uniform magnetic field B in the z -direction (perpendicular to the plane of the lattice), and the phase factor

becomes $\exp(iaBy)$ [with $e/(\hbar c) = 1$] [73, 95]. So, the hopping parameter t along the x -direction now becomes $t * \exp(iaBy)$, whereas it remains unchanged along the y -direction.

We consider the *particle in a box* approximation and set $V(ak, al) = 0$ in it. Following the Ref. [73], we use the Kwant code [74] and implement the quarter Sinai billiard system on a 120×75 rectangular lattice by removing a *quarter* elliptical portion from the left lower corner of it. The elliptical shape follows the equation $x^2/60^2 + y^2/50^2 = 1$. The dimension of the corresponding tight-binding matrix is 6789 and we set $a = t = 1$ throughout this calculation. In Fig. 8 (*bottom*), we present the Kwant generated image for this two-dimensional quarter Sinai billiard system. The pure *rectangular billiard* is known to be classically integrable. To compare the spectral correlations of the quantum rectangular billiard system against the chaotic quarter Sinai billiard system, we also carry out our Kwant calculations for this system on a 120×75 rectangular lattice and present the corresponding schematic in Fig. 8 (*top*). The dimension of the corresponding tight-binding matrix is 9196.

For $B = 0$ ($B \neq 0$), the time-reversal symmetry of the system is preserved (broken), the spectral correlations of the quarter Sinai billiard system are expected to follow the GOE (GUE) statistics [73]. In Fig. 9(b)-(d), we plot the nNNSD of this single-body chaotic billiard system. Fig. 9(b) represents the $B = 0$ scenario, which follows the distribution $P_{\text{GOE}}^2(w_2)$. To avoid the emergence of Landau levels and the resulting deviations from RMT behavior [73], we use a small magnetic field, $B = 0.01$, and plot the corresponding nNNSD for the billiard system in Fig. 9(d), which matches well with the distribution $P_{\text{GUE}}^2(w_2)$. In Fig. 9(c), we present an intermediate case, $B = 0.0003$, which is well described by our derived semi-analytical distribution $\mathcal{F}_\gamma(\mathfrak{s})$ with $\gamma = 0.5$. To compare with the spectral correlation statistics of the integrable system, we also calculate the nNNSD of the rectangular billiard system and plot its semi-Poissonian [$P_{\text{Poi}}^2(w_2)$] statistical behavior in Fig. 9(a).

B. Chaos in Quantum Many-body Systems with No Classical Analogue: Disordered Spin-chain Models

In this Section, we perform calculations on two disordered spin-chain models, which we refer to as model-I and model-II, already introduced in our earlier works [40, 47]. The competition between different Hamiltonian terms can break or preserve various unitary and antiunitary symmetries and therefore determine the spectral correlation statistics of the Hamiltonian matrices of these many-body correlated systems, as discussed at length in References [40, 47], in the context of NNSD and RD calculations in various regimes. In this section, we study the much less studied nNNSD’s of these systems, and com-

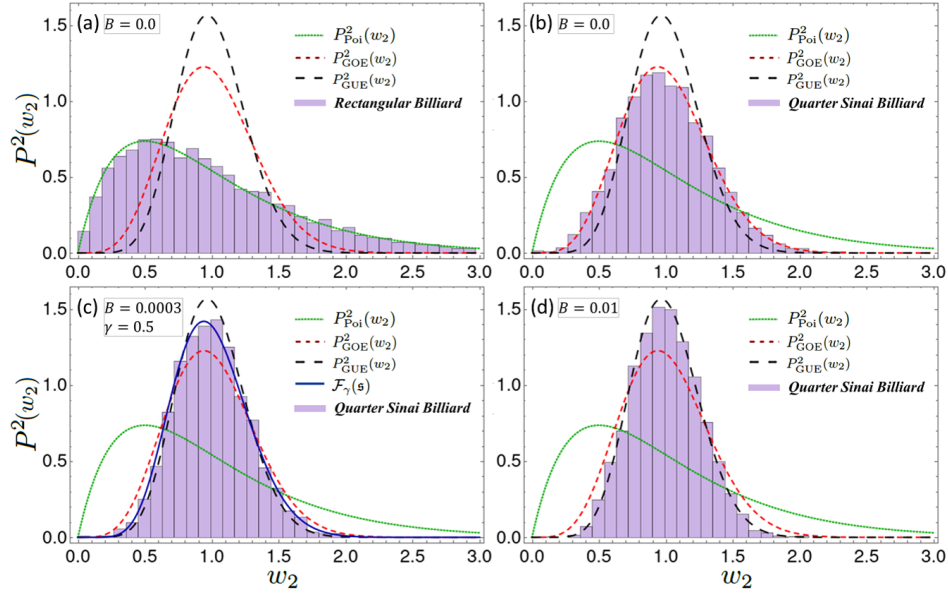


Figure 9. The nNNSD's for the single-body (a) integrable rectangular billiard and (b)-(d) chaotic quarter Sinai billiard systems. (a) Shows the semi-Poissonian statistics for the rectangular billiard with ($B = 0$ with the tight-binding matrix dimension 9196). In (b) and (d), we plot the nNNSD for the quarter Sinai billiard system (with the tight-binding matrix dimension 6789) in the GOE limit ($B = 0$) and GUE limit ($B = 0.01$), respectively. In (c), the intermediate distribution ($B = 0.0003$), in the crossover region, is perfectly mapped by our derived semi-analytical distribution $\mathcal{F}_\gamma(\mathfrak{s})$, with $\gamma = 0.5$.

pare them with the exact analytical results obtained in the previous sections.

1. Model-I

Our model-I is a one-dimensional half-filled spin- $\frac{1}{2}$ Hamiltonian, given by [40],

$$\begin{aligned}
 H_1 &= H_h + H_r + H_c \\
 &= \sum_{j=1}^{N-1} J \mathbf{S}_j \cdot \mathbf{S}_{j+1} + \sum_{j=1}^N h_j S_j^z \\
 &+ \sum_{j=1}^{N-2} J_t \mathbf{S}_j \cdot [\mathbf{S}_{j+1} \times \mathbf{S}_{j+2}], \quad (28)
 \end{aligned}$$

which has N sites with one spin per lattice site. In this model, the isotropic Heisenberg term (H_h) [97–99] is coupled to a randomly distributed and spatially inhomogeneous magnetic field by the random Zeeman term H_r . It also includes the 3-site scalar spin-chirality term H_c . This type of spin correlation term, may appear when a circularly polarized laser is used to probe Mott insulators [40, 42, 46, 100, 101]. Here \mathbf{S}_j is the vector spin operator at site j , and J is the nearest-neighbor exchange interaction. Disorder is introduced in the Zeeman term via the parameter h_j , a random magnetic field along z-direction at site j , drawn from a Gaussian distribution having zero mean and variance h^2 . J_t is the coupling constant, which appears in the three-site scalar spin-chirality term H_c .

For constructing the Hamiltonian matrix, we consider a direct product basis of single-site spin- $1/2$'s. Each site can occupy either of an up-spin ($m^z = 1/2 \equiv \uparrow$) or a down-spin ($m^z = -1/2 \equiv \downarrow$), with m^z being the eigenvalue of the z-component of the spin operator S^z . There exists 2^N number of basis states ($|m_1^z m_2^z m_3^z \dots m_N^z\rangle$) for an N -site system. $S^z = \sum_{j=1}^N S_j^z$ is the z-component of the total spin and we find that $[S^z, H_1] = 0$. H_1 consists of irreducible blocks corresponding to different S^z subsectors. As a result, the eigenvalues of these subsectors are not correlated, whereas the eigenvalues within a given sector are correlated. For RMT analysis consideration, we need to work with one such block. In our calculations, we consider an *even* N and the $S^z = 0$ subsector (Hilbert space dimension $n = C_{N/2}^N$). Throughout the paper, we set $J = 1$. The sign of J does not affect the calculations involving the entire spectrum, which is obtained from the full *exact diagonalization* methods [40]. By varying the physical crossover parameters h and J_t , the *conventional* and *unconventional* time-reversal symmetries are systematically broken, we can achieve the Poissonian, GOE, and GUE statistics and crossovers amongst them (for details see the Ref. [40]).

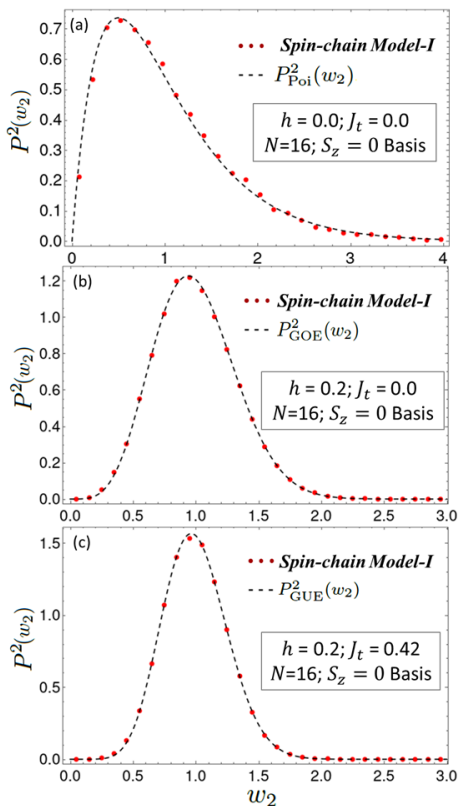


Figure 10. The nNNSD of the spin-chain model-I ($N = 16$ system). (a) represents the integrable limit ($h = 0.0$ and $J_t = 0.0$), which follows the semi-Poissonian statistics [$P_{\text{Poi}}^2(w_2)$ in Table II]. (b) and (c) represent the GOE ($h = 0.2$ and $J_t = 0.0$) and the GUE ($h = 0.2$ and $J_t = 0.42$) limits, and follow the Wigner-surmise-like results, $P_{\text{GOE}}^2(w_2)$ and $P_{\text{GUE}}^2(w_2)$ (listed in Table II), respectively.

2. Model-II

Model-II is represented by another half-filled, N site, one-dimensional spin- $\frac{1}{2}$ Hamiltonian H_2 , given by [47]

$$\begin{aligned}
 H_2 &= H_h + H_{ir} + H_r + H_{DM} \\
 &= \sum_{j=1}^{N-1} J \mathbf{S}_j \cdot \mathbf{S}_{j+1} + \sum_{j=1}^{N-1} J \epsilon_j S_j^z S_{j+1}^z \\
 &\quad + \sum_{j=1}^N h_j S_j^z + \sum_{j=1}^{N-1} \mathbf{D} \cdot [\mathbf{S}_j \times \mathbf{S}_{j+1}]. \quad (29)
 \end{aligned}$$

Among the four terms of this spin-chain Hamiltonian, H_h and H_r also appear in model-I. H_{ir} is the second random term in model-II, which is called the random *Ising* term, where the exchange interaction is randomized by multiplying J with the dimensionless random parameter ϵ_j , which follows a Gaussian distribution having zero mean and variance ϵ^2 . In a real system this could arise from a randomly varying lattice spacing due to quenched disorder, and a resultant random superexchange coupling between neighboring spins. H_{DM} is the well known anti-

symmetric *Dzyaloshinskii-Moriya* (DM) interaction term [102–106], describing the anisotropic effective spin-spin coupling between the neighboring spins. While competing with the Heisenberg term, the anti-symmetric spin part, $(\mathbf{S}_j \times \mathbf{S}_{j+1})$, results in *canted spin arrangements* [107] in real materials.

Unlike H_1 , H_2 does not commute with the total S^z , in general, due to the presence of H_{DM} , so we use the full 2^N number of basis states for some of our calculations involving model-II. On the other hand, if only finite H_h and H_{ir} terms present in a system, the total S^z remains conserved, and we need to work in a constant to a S^z sector. Here we choose an *odd* value for N to ensure that our spin-1/2 chain has a doubly degenerate eigenspectrum (in full basis calculations), which is referred to as the *Kramers degeneracy* (KD). By tuning the physical crossover parameters ϵ , h , and D (all measured in units of J), we break several unitary (spin-rotational) and anti-unitary (time-reversal) symmetries, and can achieve the Poissonian and the three canonical Wigner-Dyson ensembles (for details see the Ref. [47]).

3. Methodology and Results for the Spin-chain Models

It is known that the density of states (DOS) of the RMT matrices follow the classic Wigner’s semi-circular form [25]. However, as is well known, the DOS of a quantum chaotic system follows a more Gaussian-like distribution, due to a finite range of interactions in a physical system resulting in much sparser matrices compared to the RMT ensembles. However, surprisingly, the NNSD and other short-range higher-order spectral correlations for physical systems seem to be somewhat insensitive to this difference between physical systems and RMT, and show excellent agreement between the RMT predictions (Wigner-surmises) and the corresponding distributions from non-interacting as well as interacting many-body systems [40, 42, 47, 79, 93, 108, 109]. As far as the nNNSD is concerned, we have already seen that the RMT predicted results show very good agreement with those derived from non-interacting quantum chaotic models like the QKR or the Chaotic billiard systems. In this Section, we will discuss the comparison of the RMT based predictions to the results from the above two interacting quantum many-body models.

When studying the correlation statistics of a physical system, it is a common practice to only analyze the *mid* of the spectrum [110], where the states are closest to being ergodic. In Refs. [40] and [47], we have already shown that for a significantly large system size, we can consider the *full* spectrum and study the spectral correlation statistics of the disordered, interacting quantum systems and this is what we consider here too. Before studying the nNNSD, we perform standard unfolding [25, 40, 47] of the spectrum to eliminate any dependence on system-specific level-density.

To check the robustness of the Wigner-surmise-like

nNNSD results obtained from the RMT matrix models in Sec. II, we want to compare them against the corresponding nNNSD's of the eigenspectra from both the interacting quantum spin models (model-I and model-II). In the integrable limit ($h = 0.0$ and $J_t = 0.0$ [40]) of the $N = 16$ system ($S^z = 0$ sector), following the model-I Hamiltonian [Eq. (28)], we compare its nNNSD with the RMT predicted semi-Poissonian statistics [$P_{\text{Poi}}^2(w_2)$] and plotted in Fig. 10(a). The nNNSD of model-I shows very good agreement with the RMT prediction.

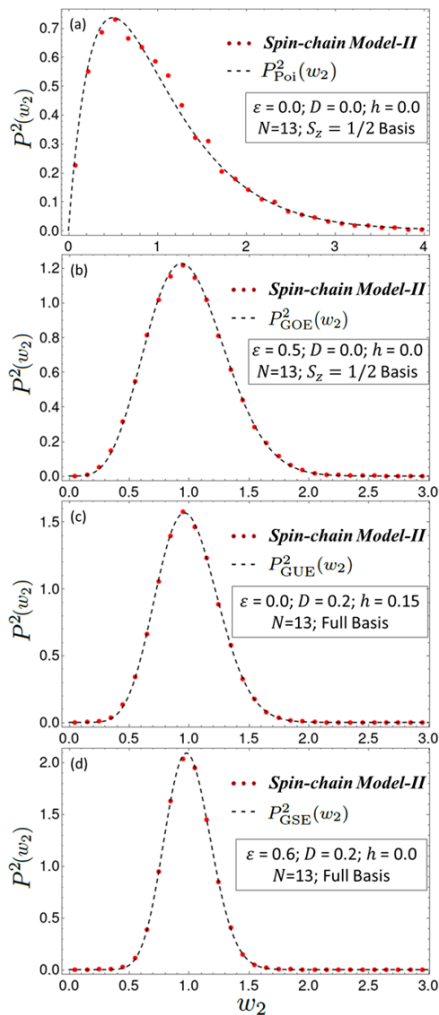


Figure 11. The nNNSD of the spin-chain model-II ($N = 13$ system) at the GSE limit ($\varepsilon = 0.6$ and $D = 0.2$ [47]), which follows the corresponding Wigner-surmise-like statistics [$P_{\text{GSE}}^2(w_2)$ in Table II].

In Fig. 10(b), we compare the nNNSD of the model-I at the GOE regime ($h = 0.2$ and $J_t = 0.0$ for $N = 16$ system in the $S^z = 0$ sector [40]) against the Wigner-surmise-like distribution $P_{\text{GOE}}^2(w_2)$. Again, for the $N = 16$ system ($S^z = 0$ sector), model-I achieves the GUE distribution at $h = 0.2$ and $J_t = 0.42$ [40]. The nNNSD of the eigenspectrum is compared with the corresponding distribution $P_{\text{GUE}}^2(w_2)$ and plotted in Fig. 10(c).

The NNSD of the model-II Hamiltonian [Eq. (29)] with $N = 13$, follows the standard GSE distribution at $\varepsilon = 0.6$, $D = 0.2$, and $h = 0.0$ (full basis) [47]. After removing the Kramers degeneracy from the eigenspectrum, we compare the calculated nNNSD with the previously obtained Wigner-surmise-like distribution $P_{\text{GSE}}^2(w_2)$, and plot them in Fig. 11(d). GUE is achieved in a scenario when both *conventional* and *unconventional* time-reversal symmetries are broken, *i.e.*, at $\varepsilon = 0.0$, $D = 0.2$, and $h = 0.15$ [47], the corresponding nNNSD is plotted in Fig. 11(c). For the completeness of our studies involving the model-II, we also plot the nNNSD of the semi-Poissonian [Fig. 11(a)] and the GOE statistics [Fig. 11(b)], achieved at $\varepsilon = 0.0$ and $\varepsilon = 0.5$ (fixed $D = 0.0$ and $h = 0.0$) [47], respectively, while working in the $S^z = 1/2$ sector.

The excellent agreements between the nNNSD's of the single- and many-body quantum chaotic systems (QKR, Sinai billiard, and spin-chain models I and II; illustrated in Figs. 7, 9, 10, and 11, respectively) and the deduced nNNSD results (as presented in Table II), conclusively demonstrate that the standard Gaussian random matrix ensembles (GOE, GUE, and GSE) effectively capture the short-range spectral correlation statistics of the quantum chaotic systems.

V. INTERESTING FEATURES IN GOE-TO-GUE AND GSE-TO-GUE CROSSOVERS

In this section, we explore two distinct crossovers in the nNNSD domain: one transitioning from the GOE to the GUE, and the other from the *non-standard* or *diluted* GSE (as discussed in reference [47]) to the GUE, using both crossover matrix models and the above spin-chain models. Additionally, the striking similarities between these two crossovers are discussed.

1. GOE-to-GUE Crossover in nNNSD

At first, we consider the crossover matrix model for the GOE-to-GUE crossover, $\mathcal{H}_{\text{GOE-GUE}}$ [Eq. (17)] with dimension $n = 12870$ (chosen to mimic the dimension of the relevant subspace in our spin model, see below) and an ensemble of $\mathcal{M} = 5$ matrices, to study the crossover in nNNSD. In Fig. 12, we plot the nNNSD for increasing *effective* crossover parameter γ' of this large n matrix model (different from the crossover parameter γ for a 3×3 matrix). Now it so turns out that the nNNSD for the GOE class and the NNSD for the GSE class possess equivalent statistical behavior [25], so we can effectively observe the crossover between two distinct spectral correlation statistics (nNNSD and NNSD) by tuning the crossover parameter γ' . In Fig. 12(a)-(d), we trace this crossover by fitting with the semi-analytical interpolating distribution $\mathcal{F}_{\gamma}(\mathfrak{s})$ (derived using the 3×3 dimensional crossover matrix model in Sec. III B) with increasing

values of the RMT crossover parameter γ , and compare against the effective crossover parameter γ' . We observe that at the GUE crossover, the parameter $\gamma \sim 1$, whereas γ' takes a much smaller value 0.03. The extreme differences in the values of the two crossover parameters (γ and γ') are expected due to scaling effects arising from the differences in their parent matrix dimensions, 3 and 12870, respectively, as previously observed in Ref. [47].

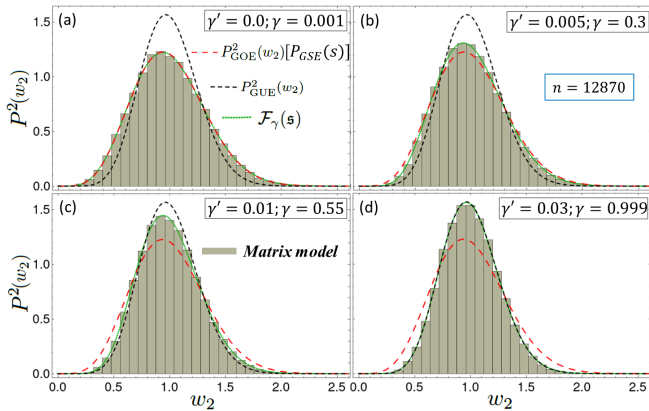


Figure 12. The nNNSD of the standard GOE-to-GUE crossover for the corresponding matrix model $\mathcal{H}_{\text{GOE-GUE}}$ [Eq. (17)], with a large dimension $n = 12870$ (ensemble of $\mathcal{M} = 5$ matrices). We also observe that, the standard nNNSD of GOE, $P_{\text{GOE}}^2(w_2)$, is equivalent to the standard NNSD of GSE, $P_{\text{GSE}}(s)$ [25]. In (a)-(d), we vary the effective crossover parameter γ' from 0.0 to 0.03. The crossover is also compared against the derived semi-analytical interpolating distribution $\mathcal{F}_\gamma(s)$ with increasing crossover parameter (γ) related to the three-dimensional JPDF.

In model-I, the GOE-to-GUE crossover is achieved by tuning the amplitude of scalar chirality interaction, J_t , while keeping h fixed at the value of 0.2 throughout, originally required to clamp the system in the GOE regime. To establish the robustness of the above crossover study, in Fig. 13(a)-(d), we plot this nNNSD crossover in model-I with $N = 16$ sites, and compare the physical crossover parameter J_t against the RMT crossover parameter γ , corresponding to the semi-analytical interpolating distribution $\mathcal{F}_\gamma(s)$.

2. GSE-to-GUE Crossover in nNNSD

While studying spectral correlation statistics of the standard GSE, it is customary to remove one of the eigenvalues from each of the Kramers doublets, whereas interesting statistics is observed in the *diluted* GSE scenario, where the Kramers degeneracy is retained [47]. In this context, we investigate the nNNSD crossover between the *diluted* GSE and the standard GUE symmetry classes. To study this crossover, we consider the corresponding form of the crossover matrix model of Eq. (16),

$$\mathcal{H}_{\text{GSE-GUE}} = \sqrt{1 - \gamma'^2} \mathcal{H}_{\text{GSE}} + \gamma' \mathcal{H}_{\text{GUE}}, \quad (30)$$

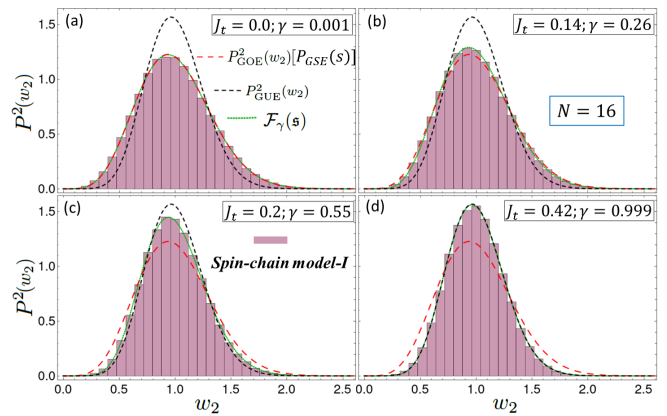


Figure 13. The nNNSD of the standard GOE-to-GUE crossover for the disordered spin model-I with $N = 16$ ($n = 12870$). In (a)-(d), we vary the physical crossover parameter J_t from 0.0 to 0.42, by keeping h fixed at 0.2 [40]. The crossover is also compared against the derived semi-analytical interpolating distribution $\mathcal{F}_\gamma(s)$ with increasing crossover parameter (γ) related to the three-dimensional JPDF.

with $n = 8192$ and an ensemble of $\mathcal{M} = 10$ matrices, where γ' is the *effective* crossover parameter for such a large matrix dimension. We observe that, in the limit $\gamma' = 0.0$, the nNNSD of the *diluted* GSE, denoted as $P_{\text{GSE}}^{KD}(w_2)$, follows the NNSD of the *standard* GSE, $P_{\text{GSE}}(s)$ [Figs. 14(a)]. This is to be expected, as we do not encounter the zero spacings from the Kramers doublets while studying the next nearest-neighbor spacings in the GSE regime [47]. Now, for a finite γ' , the KD is lifted from the eigenspectrum, and by increasing γ' , we study the GSE-to-GUE crossover in nNNSD [Figs. 14(b)-(d)]. At $\gamma' = 0.05$ [Fig. 14(d)], we observe that the distribution follows the nNNSD of the GUE, $P_{\text{GUE}}^2(w_2)$. Therefore, by varying the parameter γ' in the GSE-to-GUE crossover, we are able to demonstrate a transition from one RMT correlation study, the NNSD, to another, the nNNSD. We also plot the semi-analytical interpolating distribution $\mathcal{F}_\gamma(s)$ (discussed in Sec. III B), and compare the two crossover parameters γ' and γ . Similar to the GOE-to-GUE crossover scenario, in this case as well, we witness a substantial disparity in the values of the two crossover parameters, owing to analogous matrix dimension considerations.

To establish the generality of this interesting crossover, we investigate a similar crossover in our spin-chain model-II with lattice size $N = 13$. Now, without removing KD from the spectra, we plot the nNNSD of the system in the *diluted* GSE limit ($\epsilon = 0.6$, $D = 0.2$, and $h = 0.0$ from the Ref. [47]) in Fig. 15(a). As expected, it is identical to the standard NNSD $P_{\text{GSE}}(s)$. For any finite h , the KD is lifted, and we study the *diluted* GSE-to-GUE crossover in nNNSD, by tuning h [Figs. 15(b)-(d)]. At $h = 0.015$ [same value at which NNSD crossover is observed in Ref. [47]], we achieve the nNNSD of GUE [Fig.

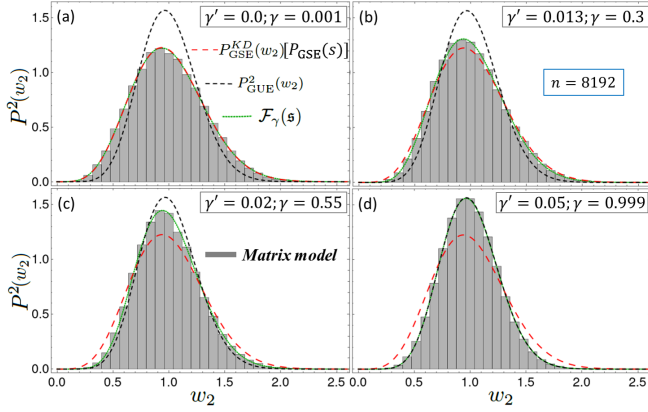


Figure 14. The nNNSD crossover between the *diluted* GSE and the standard GUE for the corresponding matrix model $\mathcal{H}_{\text{GSE-GUE}}$ [Eq. (17)], with a large dimension $n = 8192$ (ensemble of $\mathcal{M} = 10$ matrices). We observe that, at the GSE limit, the *diluted* nNNSD, $P_{\text{GSE}}^{KD}(w_2)$, is equivalent to the standard NNSD $P_{\text{GSE}}(s)$. In (a)-(d), we vary the effective crossover parameter γ' from 0.0 to 0.05. The crossover is also compared against the derived semi-analytical interpolating distribution $\mathcal{F}_\gamma(\mathfrak{s})$ with increasing crossover parameter (γ) related to the three-dimensional JPDF.

15(d)]. In Fig. 15, we observe that the semi-analytical interpolating distribution $\mathcal{F}_\gamma(\mathfrak{s})$, which is characterized by an increasing RMT crossover parameter γ , effectively captures the limiting and intermediate cases of this physical crossover. Also, a comparison is drawn between the values of the physical symmetry-breaking parameter h and the RMT crossover parameter γ .

Although both of these nNNSD crossovers (the transition from the standard GOE to the standard GUE and from the diluted GSE to the standard GUE), exhibit distinct symmetry settings corresponding to the two distinct spin-chain models, it is noteworthy that, they can be conceptualized in terms a unified mathematical expression for the distribution functions that characterize the effective RMT transitions. This understanding arises from the fact that, the behavior of nNNSD in the standard GOE regime effectively mirrors the NNSD of the standard GSE [25]. Additionally, this equivalence holds true when considering every *second* eigenvalue for calculating the NNSD (or effectively the nNNSD) in the case of the *diluted* GSE. Thus, both crossovers start from a statistically equivalent point and eventually propagate to the standard GUE regime. Based on the analysis of the Figs. 12 and 14, it is evident that the effective crossover parameters γ' associated with large-dimensional ($n = 12870$ and 8192 , respectively) crossover matrix models is considerably smaller than the corresponding crossover parameters γ , linked to the semi-analytical interpolating distribution $\mathcal{F}_\gamma(\mathfrak{s})$, based on 3×3 matrix models. The observed phenomenon aligns with the understanding presented in the Refs. [24, 40, 111] that, as the matrix dimensions increase (linked monotonically to the size of a physical system, for physical Hamiltonians), a smaller

crossover parameter value can induce a transition from one RMT ensemble to another, thus gradually abolishing the lag seen in the symmetry-breaking, as a function of the mixing or symmetry-breaking parameter, for finite systems.

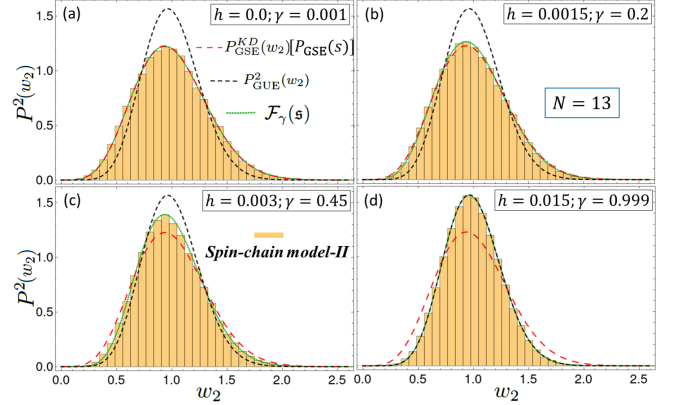


Figure 15. The nNNSD crossover between the *diluted* GSE and the standard GUE for the disordered spin model-II with $N = 13$ ($n = 8192$ and $\mathcal{M} = 10$). We observe that, at the GSE limit, the *diluted* nNNSD, $P_{\text{GSE}}^{KD}(w_2)$, is equivalent to the standard NNSD $P_{\text{GSE}}(s)$. In (a)-(d), we vary the physical crossover parameter h from 0.0 to 0.015 by keeping fixed parameters at $\epsilon = 0.6$ and $D = 0.2$ [47]. The crossover is also compared against the derived semi-analytical interpolating distribution $\mathcal{F}_\gamma(\mathfrak{s})$ with increasing crossover parameter (γ) related to the three-dimensional JPDF.

VI. CONCLUSIONS

In this paper, we have explored the *Wigner-surmise-like* and *exact analytical* results for the next-nearest-neighbor spacing distributions associated with random matrix models, whose spectral correlation statistics belong to the integrable class (semi-Poissonian) or various Wigner-Dyson symmetry classes (GOE, GUE, and GSE). The extended-Wigner-surmise results were deduced by stringent fittings to relevant spectral fluctuation statistics of large random matrices with appropriate symmetries. On the other hand, the exact analytical results for the GOE and GUE classes were derived by considering the joint probability density of eigenvalues from the 3×3 matrix models. Moreover, using the analytical expression of the JPDF for the GOE-to-GUE crossover, we have derived the corresponding semi-analytical distribution that interpolates between GOE and GUE nNNSD's. Our study also involved examining the concurrence between our nNNSD results and the spectral statistics of both single-body (QKR and QQSB) and many-body (spin-chain model-I and model-II) quantum chaotic systems. The key findings of this paper are listed below:

(1) Our findings reveal that the effective Dyson indices (β') associated with the nNNSD exhibit a robust behavior, in the sense that the β' values depend solely on the

Wigner-Dyson symmetry classes, rather than on the specific statistical measures of correlation, such as nNNSD or *second order* RD.

(2) The *Wigner-surmise-like* nNNSD results thus obtained, accurately capture the spectral correlation statistics of the studied quantum chaotic systems, *viz.* the single-body Quantum Kicked Rotor and Quantum Billiard systems, as well as the many-body disordered spin-chain model-I and model-II, both in the *integrable* and the *quantum chaotic* limits.

(3) The *exact analytical* nNNSD results, obtained from the three-dimensional joint probability density of eigenvalues for the GOE and the GUE, demonstrate a harmonious correspondence with the semi-Poissonian or the Wigner-surmise-like nNNSD findings, as well as with the corresponding nNNSD of the single-body and many-body quantum chaotic systems, in the *integrable* and the *chaotic* limits, respectively. This, in a way, validates the BGS and the Berry-Tabor conjectures for the nNNSD, going beyond NNSD.

(4) The variations of the derived crossover semi-analytical nNNSD form $[\mathcal{F}_\gamma(\mathfrak{s})]$, interpolating between the GOE and the GUE, as a function of the crossover parameter γ , show excellent agreement with the transition between the two limiting cases (GOE and GUE), be

it in the case of higher dimensional matrix models, or the single-body and many-body physical models, discussed in this paper.

(5) Finally, our analysis of two interesting nNNSD crossovers, the GOE-to-GUE transition and the *diluted* GSE-to-GUE transition, in the context of both crossover matrix models and the above two interacting spin models (model-I and model-II), shows that both of these can be alternately viewed as crossovers between the NNSD of an alternate statistics (the *standard* GSE) and the nNNSD of the GUE, as far as their mathematical forms are concerned.

ACKNOWLEDGMENTS

D.K. and S.S.G. acknowledge the Science and Engineering Research Board (SERB), Department of Science and Technology (DST), Government of India, for financial support via Project No. ECR/2016/002054. S.K. acknowledges financial support provided by SERB, DST, Government of India, via Project No. CRG/2022/001751. D.K. acknowledges Ashutosh Dheer for his assistance in gaining proficiency with the Kwant package.

Appendix A: Derivation of nNNSD for GOE and GUE from Three-dimensional JPDF's

In this appendix, we consider the three-dimensional joint probability densities of the Gaussian Orthogonal and Gaussian Unitary matrix ensembles and following the similar methods implemented in the Refs. [20–22], we derive the exact nNNSD expressions presented Eqs. (10) and (11), which follow both the normalization and unit mean next nearest-neighbor spacing conditions. The three-dimensional joint probability densities for the GOE and GUE are given by $q_{\text{GOE}}(x_1, x_2, x_3)$ and $q_{\text{GUE}}(x_1, x_2, x_3)$, respectively, and represented as [23–25, 63],

$$q_{\text{GOE}}(x_1, x_2, x_3) = \frac{1}{48\sqrt{2}\pi v^6} e^{-\frac{1}{4v^2}(x_1^2+x_2^2+x_3^2)} |(x_1 - x_2)(x_1 - x_3)(x_2 - x_3)|, \quad (\text{A1})$$

$$q_{\text{GUE}}(x_1, x_2, x_3) = \frac{1}{768\pi^{3/2}v^9} e^{-\frac{1}{4v^2}(x_1^2+x_2^2+x_3^2)} [(x_1 - x_2)(x_1 - x_3)(x_2 - x_3)]^2, \quad (\text{A2})$$

where v is the corresponding scaling parameter. For convenience, we consider $v = 1$ throughout our calculations. Arranging the eigenvalues in the ascending order, $x_1 \leq x_2 \leq x_3$, we consider the next nearest-neighbor spacing as $\mathfrak{s} = x_3 - x_1$, we will impose the unit mean level spacing condition later and accordingly scale \mathfrak{s} . The corresponding probability density function for the GOE is obtained as

$$Q_{\text{GOE}}(\mathfrak{s}) = 3! \int_{-\infty}^{\infty} dx_2 \int_{-\infty}^{x_2} dx_1 \int_{x_2}^{\infty} dx_3 q_{\text{GOE}}(x_1, x_2, x_3) \delta[\mathfrak{s} - (x_3 - x_1)]. \quad (\text{A3})$$

Using the similar methods used in Refs. [60, 61, 63] for the ratio distribution, we implement the change of variables $(x_1, x_2, x_3) \rightarrow (x, x_2, y)$, by considering $x = x_2 - x_1$ and $y = x_3 - x_2$, and get

$$Q_{\text{GOE}}(\mathfrak{s}) = 6 \int_{-\infty}^{\infty} dx_2 \int_{-\infty}^{x_2} dx \int_{x_2}^{\infty} dy q_{\text{GOE}}(x_2 - x, x_2, x_2 + y) \delta[\mathfrak{s} - (x + y)]. \quad (\text{A4})$$

Using Eq. (A1), we first trivially perform the integral over x_2 and left with

$$Q_{\text{GOE}}(\mathfrak{s}) = \frac{1}{4\sqrt{6}\pi} \int_0^{\infty} dx \int_0^{\infty} dy e^{-\frac{(x^2+xy+y^2)}{6}} xy(x+y) \delta[\mathfrak{s} - (x+y)]. \quad (\text{A5})$$

Now, performing the integrals over y and x , we get the probability density

$$Q_{\text{GOE}}(\mathfrak{s}) = \frac{1}{16\sqrt{6\pi}} \exp(-\mathfrak{s}^2/6) \mathfrak{s} \left(12\mathfrak{s} + \exp(\mathfrak{s}^2/24) \sqrt{6\pi} (\mathfrak{s}^2 - 12) \operatorname{erf} \left[\frac{\mathfrak{s}}{2\sqrt{6}} \right] \right), \quad (\text{A6})$$

where $\operatorname{erf}[z] = \frac{2}{\sqrt{\pi}} \int_0^z e^{-t^2} dt$ is the *error function*. We check that, $Q_{\text{GOE}}(\mathfrak{s})$, follows the normalization condition $\int_0^\infty Q_{\text{GOE}}(\mathfrak{s}) d\mathfrak{s} = 1$, but the mean spacing is, $\int_0^\infty \mathfrak{s} Q_{\text{GOE}}(\mathfrak{s}) d\mathfrak{s} = 3\sqrt{\frac{6}{\pi}}$. After scaling \mathfrak{s} , so that the mean spacing is one, we obtain the normalized probability density for GOE as

$$\mathcal{Q}_{\text{GOE}}(\mathfrak{s}) = 3\sqrt{\frac{6}{\pi}} Q_{\text{GOE}} \left(3\sqrt{\frac{6}{\pi}} \mathfrak{s} \right) = \frac{3^4 \exp(-9\mathfrak{s}^2/\pi) \mathfrak{s} \left(6\mathfrak{s} - \exp(9\mathfrak{s}^2/4\pi) (2\pi - 9\mathfrak{s}^2) \operatorname{erf} \left[\frac{3\mathfrak{s}}{2\sqrt{\pi}} \right] \right)}{4\pi^2}. \quad (\text{A7})$$

Now, using $q_{\text{GUE}}(x_1, x_2, x_3)$ [Eq. (A2)] in the Eq. (A4) and performing similar processes, we get the normalized probability density for GUE,

$$\mathcal{Q}_{\text{GUE}}(\mathfrak{s}) = \frac{3^{11} \sqrt{3} \exp(-3^5 \mathfrak{s}^2/2^4 \pi) \mathfrak{s}^2 \left(2^3 3^3 \mathfrak{s} (-2^5 \pi + 3^4 \mathfrak{s}^2) + \sqrt{3} \exp(3^5 \mathfrak{s}^2/2^6 \pi) (2^{10} \pi^2 - 2^6 3^4 \pi \mathfrak{s}^2 + 3^9 \mathfrak{s}^4) \operatorname{erf} \left[\frac{9}{8} \sqrt{\frac{3}{\pi}} \mathfrak{s} \right] \right)}{2^{20} \pi^4}, \quad (\text{A8})$$

which also follows the unit mean nearest-neighbor spacing condition. It is to note that, after scaling, the spacing parameter \mathfrak{s} , formally becomes equivalent to the parameter w_2 .

- [1] F. Haake, S. Gnutzmann, and M. Kuś, *Quantum Signatures of Chaos* (Springer, Cham, 2018).
- [2] L. E. Reichl, *The Transition to Chaos: Conservative Classical Systems and Quantum Manifestations* (Springer, New York, 2004).
- [3] L. E. Stöckmann, *Quantum Chaos: An Introduction* (Cambridge University Press, Cambridge, 2007).
- [4] Edward Ott, *Chaos in Dynamical Systems* (Cambridge University Press, Cambridge, 2002).
- [5] Kathleen T. Alligood, Tim D. Sauer, and James A. Yorke, *Chaos: An Introduction to Dynamical Systems* (Springer-Verlag, New York, 1996).
- [6] Stefan Weigert, *Physica D* **56**, 107 (1992); Jean-Sébastien Caux and Jorn Mossel, *J. Stat. Mech.* (2011) P02023.
- [7] M. V. Berry and M. Tabor, *Proc. R. Soc. Lond. A* **356**, 375 (1977).
- [8] O. Bohigas, M. J. Giannoni, and C. Schmit, *Phys. Rev. Lett.* **52**, 1 (1984).
- [9] F. J. Dyson, *J. Math. Phys.* **3**, 140 (1962).
- [10] F. J. Dyson, *J. Math. Phys.* **3**, 1199 (1962).
- [11] E. P. Wigner, *Proc. Camb. Philos. Soc.* **47**, 790 (1951).
- [12] E. P. Wigner, *Gathnberg Conference on Neutron Physics by Time-of-Flight* (Oak-Ridge National Laboratory Report No. 2309, US, 1957) p. 59.
- [13] E. P. Wigner, *Statistical Properties of Real Symmetric Matrices with Many Dimensions* (Princeton University Press, Princeton, NJ, 1957) pp. 188–198.
- [14] E. P. Wigner, *Ann. Math.* **62**, 548 (1955).
- [15] E. P. Wigner, *Ann. Math.* **65**, 203 (1957).
- [16] E. P. Wigner, *Ann. Math.* **67**, 325 (1958).
- [17] E. P. Wigner, *SIAM Rev.* **9**, 1 (1967).
- [18] M. L. Mehta, *Nucl. Phys.* **18**, 395 (1960).
- [19] F. J. Dyson, *J. Math. Phys.* **3**, 1191 (1962).
- [20] C. E. Porter, *Nucl. Phys.* **40**, 167 (1963).
- [21] P. B. Kahn and C. E. Porter, *Nucl. Phys.* **48**, 385 (1963).
- [22] C. E. Porter, *Statistical Theories of Spectra: Fluctuations*, Perspectives in Physics : a series of reprint collections (Academic Press, New York, 1965).
- [23] M. L. Mehta and A. Pandey, *J. Phys. A: Math. Gen.* **16**, 2655 (1983).
- [24] A. Pandey and M. L. Mehta, *Commun. Math. Phys.* **87**, 449 (1983).
- [25] M. L. Mehta, *Random Matrices*, Pure and Applied Mathematics (Elsevier Science, Netherlands, 2004).
- [26] F. J. Dyson and M. L. Mehta, *J. Math. Phys.* **4**, 701 (1963).
- [27] M. L. Mehta and F. J. Dyson, *J. Math. Phys.* **4**, 713 (1963).
- [28] T. Guhr, A. Muller-Groeling, and H. A. Weidenmuller, *Phys. Rep.* **299**, 189 (1998).
- [29] C. W. J. Beenakker, *Rev. Mod. Phys.* **69**, 731 (1997).
- [30] Y. Alhassid, *Rev. Mod. Phys.* **72**, 895 (2000).
- [31] V. Plerou, P. Gopikrishnan, B. Rosenow, L. A. Nunes Amaral, and H. E. Stanley, *Phys. Rev. Lett.* **83**, 1471 (1999).
- [32] M. S. Santhanam and P. K. Patra, *Phys. Rev. E* **64**, 016102 (2001).
- [33] P. Seba, *Phys. Rev. Lett.* **91**, 198104 (2003).
- [34] I. J. Farkas, I. Derényi, A.-L. Barabási, and T. Vicsek, *Phys. Rev. E* **64**, 026704 (2001).
- [35] G. Jafari, A. H. Shirazi, A. Namaki, and R. Raei, *Comput. Sci. Eng.* **13**, 84 (2011).
- [36] F. Luo, J. Zhong, Y. Yang, R. H. Scheuermann, and J. Zhou, *Phys. Lett. A* **357**, 420 (2006).
- [37] A. Kikkawa, *Sci. Rep.* **8**, 10607 (2018).

- [38] G. Akemann, J. Baik, and P. D. Francesco, eds., *Handbook of Random Matrix Theory* (Oxford University Press, Oxford, 2011).
- [39] C. P. Dettmann, O. Georgiou, and G. Knight, *EPL* **118**, 18003 (2017).
- [40] D. Kundu, S. Kumar, and S. Sen Gupta, *Phys. Rev. B* **105**, 014205 (2022).
- [41] A. Y. Abul-Magd and M. H. Simbel, *Phys. Rev. E* **60**, 5371 (1999).
- [42] Y. Avishai, J. Richert, and R. Berkovits, *Phys. Rev. B* **66**, 052416 (2002).
- [43] M. Collura, H. Aufderheide, G. Roux, and D. Karevski, *Phys. Rev. A* **86**, 013615 (2012).
- [44] N. Chavda and V. Kota, *Phys. Lett. A* **377**, 3009 (2013).
- [45] S. Iyer, V. Oganessian, G. Refael, and D. A. Huse, *Phys. Rev. B* **87**, 134202 (2013).
- [46] R. Modak and S. Mukerjee, *New J. Phys.* **16**, 093016 (2014).
- [47] D. Kundu, S. Kumar, and S. Sen Gupta, *Phys. Rev. B* **107**, 094205 (2023).
- [48] M. S. Santhanam and P. K. Patra, *Phys. Rev. E* **64**, 016102 (2001).
- [49] A. Pandey, S. Puri, and S. Kumar, *Phys. Rev. E* **71**, 066210 (2005).
- [50] S. Jalan and J. N. Bandyopadhyay, *Phys. Rev. E* **76**, 046107 (2007).
- [51] S. M. Abuelenin and A. Y. Abul-Magd, *Procedia Comput. Sci.* **12**, 69 (2012).
- [52] C. L. Bertrand and A. M. García-García, *Phys. Rev. B* **94**, 144201 (2016).
- [53] J. M. G. Gómez, R. A. Molina, A. Relaño, and J. Retamosa, *Phys. Rev. E* **66**, 036209 (2002).
- [54] M. M. Duras and K. Sokalski, *Phys. Rev. E* **54**, 3142 (1996).
- [55] D. Engel, J. Main, and G. Wunner, *J. Phys. A: Math. Gen.* **31**, 6965 (1998).
- [56] S. H. Tekur, U. T. Bhosale, and M. S. Santhanam, *Phys. Rev. B* **98**, 104305 (2018).
- [57] P. Rao, M. Vyas, and N. D. Chavda, *Eur. Phys. J.: Spec. Top.* **229**, 2603 (2020).
- [58] W.-J. Rao, *Phys. Rev. B* **102**, 054202 (2020).
- [59] U. T. Bhosale, *Phys. Rev. B* **104**, 054204 (2021).
- [60] Y. Y. Atas, E. Bogomolny, O. Giraud, and G. Roux, *Phys. Rev. Lett.* **110**, 084101 (2013).
- [61] Y. Y. Atas, E. Bogomolny, O. Giraud, P. Vivo, and E. Vivo, *J. Phys. A: Math. Theor.* **46**, 355204 (2013).
- [62] S. H. Tekur, S. Kumar, and M. S. Santhanam, *Phys. Rev. E* **97**, 062212 (2018).
- [63] A. Sarkar, M. Kothiyal, and S. Kumar, *Phys. Rev. E* **101**, 012216 (2020).
- [64] E. B. Bogomolny, U. Gerland, and C. Schmit, *Phys. Rev. E* **59**, R1315 (1999).
- [65] U. T. Bhosale, *Phys. Rev. E* **107**, 024132 (2023).
- [66] F. M. Izrailev, *Phys. Rev. Lett.* **56**, 541 (1986).
- [67] G. Casati and L. Molinari, *Prog. Theor. Phys. Supp.* **98**, 287 (1989).
- [68] F. M. Izrailev, *Physics Reports* **196**, 299 (1990).
- [69] A. B. Jaiswal, A. Pandey, and R. Prakash, *EPL* **127**, 30004 (2019).
- [70] A. Kumar, A. Pandey, and S. Puri, *Phys. Rev. E* **101**, 022218 (2020).
- [71] Y. G. Sinai, *Dokl. Akad. Nauk SSSR* **153**, 1261 (1963).
- [72] Y. G. Sinai, *Russ. Math. Surv.* **25**, 137 (1970).
- [73] R. S. Chandramouli, R. K. Srivastav, and S. Kumar, *Chaos* **30**, 123120 (2020).
- [74] C. W. Groth, M. Wimmer, A. R. Akhmerov, and X. Waintal, *New J. Phys.* **16**, 063065 (2014).
- [75] The NNSD of integrable systems follow Poissonian statistics, but the higher-order spacing distributions (like nNNSD here) do not follow Poissonian statistics, and in general, referred to as semi-Poissonian distributions [58, 64]. The nomenclature arises from the observation that, the NNSD of a new sequence $\{\tilde{\varepsilon}'_j\}$, obtained by averaging neighboring elements $[\tilde{\varepsilon}'_j = (\tilde{\varepsilon}_j + \tilde{\varepsilon}_{j+1})/2]$ from an ordered Poissonian distributed sequence $(\tilde{\varepsilon}_1 \leq \dots \leq \tilde{\varepsilon}_j \leq \tilde{\varepsilon}_{j+1} \leq \dots)$, follows the semi-Poissonian distribution $P_{\text{Poi}}^2(w_2)$.
- [76] G. Lenz and F. Haake, *Phys. Rev. Lett.* **65**, 2325 (1990).
- [77] B. V. Chirikov, *Research concerning the theory of nonlinear resonance and stochasticity* (CERN, Geneva, 1971) translated at CERN from the Russian (IYAF-267-TRANS-E).
- [78] A. Lichtenberg and M. Leiberman, *Regular and Stochastic Motion*, Applied Mathematical Sciences (Springer New York, 2013).
- [79] M. Santhanam, S. Paul, and J. B. Kannan, *Phys. Rep.* **956**, 1 (2022).
- [80] F. M. Izrailev, *Phys. Lett. A* **134**, 13 (1988).
- [81] A. Pandey, R. Ramaswamy, and P. Shukla, *Pramana* **41**, L75 (1993).
- [82] P. Shukla and A. Pandey, *Nonlinearity* **10**, 979 (1997).
- [83] G. Casati, I. Guarneri, F. Izrailev, and R. Scharf, *Phys. Rev. Lett.* **64**, 5 (1990).
- [84] Y. V. Fyodorov and A. D. Mirlin, *Phys. Rev. Lett.* **67**, 2405 (1991).
- [85] For the integrable case, the parameter α is varied from 11 to 30 and for the chaotic case, it is varied from 20,001 to 20,020, to construct the matrix ensembles..
- [86] V. Lopac, I. Mrkonjić, and D. Radić, *Phys. Rev. E* **59**, 303 (1999).
- [87] L. A. Bunimovich, *Funct. Anal. Appl.* **8**, 254 (1974).
- [88] L. A. Bunimovich, *Commun. Math. Phys.* **65**, 295 (1979).
- [89] E. Cuevas, E. Louis, and J. A. Vergés, *Phys. Rev. Lett.* **77**, 1970 (1996).
- [90] B. Dietz, T. Klaus, M. Miski-Oglu, A. Richter, M. Wunderle, and C. Bouazza, *Phys. Rev. Lett.* **116**, 023901 (2016).
- [91] K. Frahm and J.-L. Pichard, *J. Phys. I France* **5**, 877 (1995).
- [92] L. Huang, Y.-C. Lai, and C. Grebogi, *Chaos: An Interdisciplinary Journal of Nonlinear Science* **21**, 013102 (2011).
- [93] V. K. B. Kota, *Embedded Random Matrix Ensembles in Quantum Physics* (Springer, Cham, 2014).
- [94] P. Yu, Z.-Y. Li, H.-Y. Xu, L. Huang, B. Dietz, C. Grebogi, and Y.-C. Lai, *Phys. Rev. E* **94**, 062214 (2016).
- [95] R. Peierls, *Z. Phys.* **80**, 763 (1933).
- [96] D. R. Hofstadter, *Phys. Rev. B* **14**, 2239 (1976).
- [97] W. Heisenberg, *Z. Physik* **49**, 619 (1928).
- [98] F. Bloch, *Z. Physik* **61**, 206 (1930).
- [99] F. Bloch, *Z. Physik* **74**, 295 (1932).
- [100] D. Sen and R. Chitra, *Phys. Rev. B* **51**, 1922 (1995).
- [101] S. Kitamura, T. Oka, and H. Aoki, *Phys. Rev. B* **96**, 014406 (2017).
- [102] T. Moriya, *Phys. Rev. Lett.* **4**, 228 (1960).
- [103] T. Moriya, *Phys. Rev.* **120**, 91 (1960).

- [104] I. Dzyaloshinsky, *J. Phys. Chem. Solids* **4**, 241 (1958).
- [105] R. Hamazaki and M. Ueda, *Phys. Rev. E* **99**, 042116 (2019).
- [106] J. Vahedi, A. Ashouri, and S. Mahdavifar, *Chaos* **26**, 103106 (2016).
- [107] K. Yosida, *Theory of Magnetism* (Springer Berlin, Heidelberg, 1996).
- [108] B. Altshuler, P. Lee, and W. Webb, eds., *Mesoscopic Phenomena in Solids* (North-Holland, Amsterdam, 1991).
- [109] A. Y. Abul-Magd, *J. Phys. A Math. Gen.* **29**, 1 (1996).
- [110] S. D. Geraedts, R. Nandkishore, and N. Regnault, *Phys. Rev. B* **93**, 174202 (2016).
- [111] S. Kumar and A. Pandey, *Ann. Phys.* **326**, 1877 (2011).